Russian Geology and Geophysics
Vol. 44, No. 11, pp. 1160-1188, 2003

Geologiya i Geofizika
UDC 551.22+552.11

AGE OF XENOLITH-BEARING BASALTS AND MANTLE EVOLUTION IN THE BAIKAL RIFT ZONE

I.V. Ashchepkov, S.V. Travin, A.I. Saprykin, L. Andre*, P.A. Gerasimov, and O.S. Khmel'nikova

United Institute of Geology, Geophysics and Mineralogy, Siberian Branch of the RAS, 3 prosp. Akad. Koptyuga, Novosibirsk, 630090, Russia
** Royal Museum of Central Africa, Tervuren, Belgium*

Five age stages of xenolith-bearing basalts of the Vitim and Khamar-Daban lava plateaus have been recognized by K-Ar dating. Thermobarometry of the basalt melts suggests deep levels of magma derivation at the initial and final stages. The *PT* paths of the melt upwelling in the period of generation of lava plateau are steeper than the *PT* paths of hydrous lavas during the initial and final periods of volcanic activity. Temperature sections for a mineral (rock) vary quickly in time. For the Vitim Plateau, three zones of melt concentration have been expressed at Stage I (18–16 Ma): 25–27 kbar, 1300–1100 °C — deformed peridotites, kaersutite-phlogopite-bearing veins; black and hybrid pyroxenites; above 22–20 kbar — Ga- and Ga-Sp-lherzolites of primitive type and anatectic pyroxenites; 16–12 kbar — Sp-lherzolites with pargasite partings and disseminated Phl. At Stage II (14–12 Ma), magma was localized at the top of the Sp-facies among lherzolites of *A*-type (with enriched Al-Sp and Px). At Stage III, magma was concentrated at the bottom of the Sp-facies of the mantle: the lower part of the column — primitive lherzolites, and the upper part, *A*-lherzolites. Stage IV is characterized by a layered mantle: 1 — high-temperature pseudogarnet, 2 — primitive and pseudogarnet lherzolites, 3 — spinel and pseudogarnet lherzolites, 4 — mixed lherzolites of primitive depleted alumina type and low-temperature iron varieties. Stage V is represented by a 3-member section: 1 — high-temperature Fe-lherzolites, 2 — garnet-spinel and spinel lherzolites, 3 — aluminous and primitive lherzolites. Peaks of Fe# at temperature sections show variations in levels of localization and concentration of magma. A similar scheme is documented for Khamar-Daban. The plume basalts whose characteristics correspond to the modal melting of primitive garnet lherzolites change their composition, remelting metasomatites and pyroxenites and coming into reaction with peridotites. Rare-earth characteristics of basalts change more quickly than the isotopic ones. The amount of the material that participated in the reaction is 2–3 orders of magnitude as great as the volume of the effused basalts, which suggests its penetration into permeable zones.

Basalt, rift zone, melting, mantle, peridotites, pyroxenites, melt, differentiation, geochemistry, thermobarometry, inductively bound mass-plasma

INTRODUCTION

In the Late Cenozoic, the plume basalt magmatism was expressed over a large territory of Eurasia and other regions of the world. In eastern [1] and northeastern Asia [2] and in the South Pacific segment [3] it is spatially joint with modern and ancient zones of subduction (Fig. 1). However, the chain of Cenozoic flood basalts from the Far Eastern continental margin through Tokinsky Stanovik [4], Udokan [5, 6], Vitim Plateau [7–9], Khamar-Daban [10], East Sayan [11] to Tuva [12] traces the microplate boundaries northward from the zone of the closure of the Mongolo-Okhotsk ocean [13]. The vast area of volcanism in Central Asia, including the Hangayn plume [13], Dariganga Plateau, and separate fields of southern Mongolia is considered a hot field [14], or Mongolian

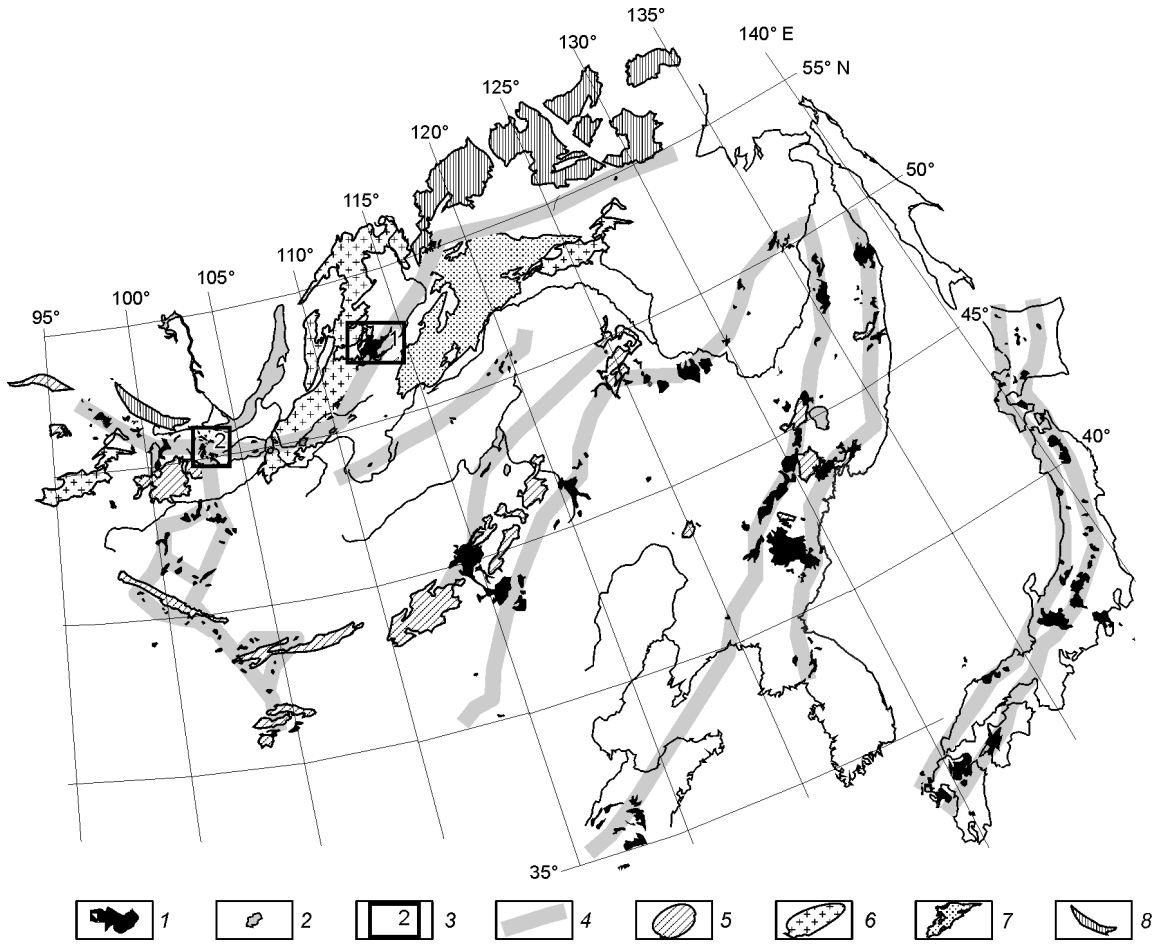

Fig. 1. Schematic location of basalt plateaus in Asia. *1* — Late Cenozoic basalt plateaus; *2* — Early Cenozoic basalts; *3* — basalt plateaus described in this paper: 1 — Vitim, 2 — Khamar-Daban; *4* — zones of basalt magmatism (ancient sutures in mantle); *5* — fragments of Paleozoic island arcs; *6* — zones of continental margin-marine magmatism; *7* — large granite batholiths; *8* — fragments of microcontinents with Precambrian crust.

superplume [15]. Its sizes (about 2000 km) are characteristic of the typical plumes (Icelandic [16], East African [17], and Hawaiian [18]). Via volcanic regions of Northern and Central China, this area joins the East Chinese field [19] (see Fig. 1). The continental and oceanic lava plateaus developed in the same way, as inferred from the evolution of chemistry of effused lavas, recurrence of volcanism, composition of mantle peridotites and pyroxenites and structure of mantle sections [1–22].

With basalt ages (Table 1) from two districts of the Baikal Rift Zone, Vitim Plateau and Khamar-Daban, we will compare the mantle columns reconstructed using hundreds of analyses of mantle-derived inclusions and trace the joint evolution of volcanism and its mantle roots.

METHODS

In K-Ar method, potassium was determined by isotope dilution from 50–100 mg specimens on an MI1201T solid-phase mass spectrometer (Sumy, Ukraine). The error of determination was no more than 1%. The argon content was also determined by isotope dilution, with ^{38}Ar used as a tracer calibrated by a standard specimen, MCA-11 biotite. Argon was isolated on an all-metal set-up with a molybdenum crucible and Ta-foil cylinder as a heater. Spongy titanium getters were used for cleaning. Measurements of isotope composition of Ar were carried out on an improved version of MI1201B gas mass spectrometer (Sumy, Ukraine) at a static mode of operation.

Table 1

K/Ar Datings of Basalts of Baikal Rift Zone

Sample	K_2O	$Ar_{rad.}$	Ar_{air}	Age, Ma	Location	Stage
				Vitim Upland		
623-15	2.188	0.123	81.6	0.81 ± 0.1	Dzhilinda River, valley flow	Stage V
307-73	2.53	0.14	78.5	0.83 ± 0.2	Yaksha-I volcano	Cinder cones of posterosional stage and associated flows
303/7	2.23	0.227	74	1.47 ± 0.1	Valley flow 1 km downstream from Yaksha River mouth	Stage IV
625-5	2.291	0.28	53	1.75 ± 0.7	Dzhilinda River, "Lherzolite site"	Posterosional valley flows in Dzhilinda River (Amalat)
421-3	1.63	0.314	54	2.76 ± 0.11	Flows in upper reaches of Dzhilinda River (Amalat)	
371-1	1.22	0.13	84.9	1.5 ± 0.3	Dzhilinda River near Kandidushka volcano, lower flow with xenoliths	
371-3	1.45	3.6	42.5	3.4 ± 0.3	Flow in Bol. Amalat River, left side 1 km downstream from Dzhilinda River mouth (Amalat)	Stage III Final stage of lava plateau formation
370	1.13	0.27	51.9	3.5 ± 0.3	Dzhilinda (Amalat) River, near mouth	
402-1	1.46	0.43	36.1	4.3 ± 0.3	Amnunda River, neck with xenoliths in left side, 2 km from mouth	
377-1	2.38	0.895	55	5.13 ± 0.2	Flow in Bol. Amalat River	
559-27	2.398	0.463	54.5	2.8 ± 0.3	Volcano north of Pilotskoe Lake	
4431-7*	1.403	0.646	44	6.6	Boreholes in upper reaches of Amnunda River	Stage IIa Lava plateau, middle—upper part
4431-3*	1.062	0.535	51	7.3		
3313-1*	1.009	0.513	61	7.34		
3313-9*	0.832	0.435	82	7.55		
4431-11*	0.959	0.633	66	9.6		Stage II Lava plateau
3313-14*	1.098	0.795	83	10.36		
3313-5*	0.965	0.712	70	10.65		
316-13	1.21	0.9	52.5	10.7 ± 0.7	Picrobasalt	Stage I
381-1	0.88	0.69	49.6	11.3 ± 1.6	Tetrakh River, flow with xenoliths	
382-11	1.53	1.28	14.3	12.0 ± 0.5		
381-12	1.53	1.52	60	14.3 ± 1		
379-1	0.66	0.63	32.7	14 ± 0.5	Upper reaches of Tetrakh River	
374-2	0.583	0.549	58	14.2 ± 2	Road excavation 100 m below quarry with picrobasalt, west slope, volcanic bombs in tuffs	
375-1	1.45	1.45	18.1	14.4 ± 0.6	Quarry near Bereya River	
374-1	0.58	0.58	54.8	15 ± 2		

Table 1 **(continued)**

Sample	K_2O	$Ar_{rad.}$	Ar_{air}	Age, Ma	Location	Stage
384-1	1.34	1.66	14.3	18 ± 1	Upper reaches of Dzhilinda (Amalat) River	Stage I Initial stage
PIK-1	1.263		29	18.5	Picrobasalt	
313-521	6.5	21.4	20	46.8 ± 4	Phlogopite from amphibole-phlogopite vein crossing garnet lherzolite of vein	Metasomatism preceding main portion of plume melts
386-1	1.91	16.6	10.2	122 ± 5	Basalt neck in Vitim River channel, 2 km downstream from Politovka Village	Mesozoic stage
390-2	1.82	16.4	5.7	126 ± 5	Tal'sha River, 40 km upstream along Vitim River from Romanovka Village	
373-6	1.82	23.39	9	176.9 ± 3	Xenolith of latite from quarry	
1040-1	1.68	3.36	19.8	29 ± 1.8	Eravnoe depression	I.N. Rezanov's specimens
Boldok-3	2.08	17.4	5.2	117 ± 3		
K-10-3	1.54	13.2	57.3	120 ± 5		
1043-2	1.61	16	8.6	138 ± 4		
Murochi-2	1.05	11.56	10.2	152 ± 4		
Murochi-1	1.68	21.4	6.4	176 ± 6		
Khamar-Daban						
AM	1.42	0.2	72.6	2.0 ± 0.3	Flow in middle part of unit at Mid-Margasan opposite Marta River	Stage IV
83-27	1.26	0.868	36.6	10 ± 0.3	Margasanskaya Sopka volcano	Stage III
604-10	0.809	0.67	32.8	11.9 ± 0.2	Flow in lower part of unit at Mid-Margasan	
97-1	1.07	1.2	34.1	16 ± 1.6	Khamar-Daban, beneath Tumusun volcano, upper quarter of section	Stage II
K-85	1.67	1.9	19	16.4 ± 0.9	Komar cover	
86-1	0.63	0.74	30.4	17 ± 0.7	Khamar-Daban, beneath Tumusun volcano, upper quarter of section	
485-8	1.33	1.69	55	18.1 ± 0.7	Khubutui River	
100-10	1.59	2.58	30	23.3 ± 0.6	Flow with xenoliths in basement of lava unit beneath Tumusun volcano	Stage I
East Sayan						
E. Sayan	0.825	0.597	29.1	10.4 ± 0.5	Zabit Plateau	
Henteyn Ridge						
630-68	1.674	0.718	38.9	6.2 ± 0.1	Burkal, welded cinder in Zharnichikha River	

The ^{40}Ar blank did not exceed $1–4 \cdot 10^{-13}$ mole (40 min at 1700 °C). The reported errors of datings and potassium contents fit a 95% confidence interval.

Microprobe analyses of minerals from peridotite mantle-derived inclusions (about 1500) were made by O.S. Khmel'nikova with a Camebax Micro probe at the UIGGM, Novosibirsk (at an accelerating voltage 20 kV, current 100 mA). Trace elements in lherzolite minerals were determined by the methods ICP MS (PQ Plasmaquard Turbo Plus) with chemical decomposition, MRAC (Tervuren, Belgium, analyst L. Andre) and LA ICP MS, UIGGM (Novosibirsk) at the Finnigan element mass spectrometer (analysts P.A. Gerasimov and A.I. Saprykin).

CHARACTERISTICS OF LAVAS

The Vitim Plateau is made up of lavas effused from several centers (type of shield volcanoes) of about 20 km across (Fig. 2, *a*) [20]. Volcanism began in the Bereya block (with higher K_2O/Na_2O in all lavas) (Fig. 3, *a*) southeast of the main effusions, migrated clockwise on the plateau and ended at the same place [21]. The picrobasalt tuffs (Stage I) are saturated in xenoliths, occasionally with amphibole or phlogopite, which are present in lava as well. Basaltic andesites of K series are associated with them. At the bottom of the plateau, flows of Hy-normalized basalts are common. Of ubiquitous occurrence are magnesian basanites (12–14 Ma) with spinel lherzolites in the center of the plateau (Tetrakh River) at depths of 200–170 m (exposures along the Tetrakh River; drilling core of the Sosnovskaya Expedition) (Stage II). The whole 200 m thick unit of alkali basalts was formed for 4 Ma (from 10.6 to 6.6 Ma) [9]: $150 \cdot 10^{-6}$ km/year, which is two or three orders of magnitude lower than the production of typical hot spots [22]. The northern part of the plateau is crowned with basanitoids dated at 4.3–2.8 Ma containing xenoliths of spinel lherzolites and chrome-diopside websterites (III) — the transition to the posterosional stage (about 5 Ma) of alkali basalts with abundant glomeroporphyritic phenocrysts. The Pliocene valley flows of basanites (1.45–1.75 Ma) (IV) are known in three segments — in the northwest along the Khoigot, Amnunda, Dzhilinda (Vitim) Rivers, along the Dzhilinda River (Amalat) in the Bereya block, and in the southeast, along the Vitim River [8], with inclusions of spinel and pseudogarnet lherzolites and pyroxenites [23]. Hydrous phases are rare to absent. The flows are related to necks and cinder cones tracing the orthogonal latitude-submeridional network of faults. The final stage of activity is marked by cinder cone volcanoes (Stage V, 1.0–0.8 Ma) in the Bereya block with xenoliths of lherzolites with kelyphytic garnet (about 5–10% of bombs). Phlogopites appear again in veinlets in lherzolites and as megacrysts.

The Khamar-Daban xenolith-bearing basalts are known in five age intervals. Lherzolite inclusions in Mg-basanites are everywhere: at the base, in the center of the plateau, beneath the Tumusun volcano (23 Ma), in the valleys of the Khubutui and Tsakirka Rivers (18.1 Ma) in the south and in the Komar cover in the north. The lava sequence beneath the Tumusun volcano is made up (from bottom to top) of Hy-normalized lavas and of alkali basalts (to 20 m) with megacrysts of anorthoclase. The alternation of subalkali and alkali basalts is completed by the formation of basanites with various cumulative and rare lherzolite inclusions (16–17 Ma) (Stage II). With a considerable gap they are overlain by tephra blankets from the Margasan (Margasanskaya Sopka) and Tumusun volcanoes (7–9 Ma) (Stage III). The posterosional flows (IV) are known on the northern (8 to 2 Ma) [11] and southern (5–3 Ma) slopes of the ridge (see Fig. 2, *b*). The cinder cone volcanoes (1.5–0.8 Ma) with diverse xenoliths are localized in the Tunka and Dzhida valleys (with amphibole and phlogopite) on the plateau margin (V). Variations in composition of the Khamar-Daban lavas are quite the same as in the Vitim Plateau (see Fig. 3, *b*).

The initial stages of volcanism for East Sayan [21, 24] coincide with those at Khamar-Daban (23 Ma), and volcanism in the Vitim Plateau parallels the volcanic activity on Udokan (16–18 Ma) [25]. Volcanism of the posterosional Pliocene-Pleistocene stage is expressed simultaneously over a vast area: in east Sayan [11]: (valley flows along the Yamata River), in the Dzhida River basin and on the Vitim Plateau along the Dzhilinda River (Amalat zone) and the rivers of Vitim and Amalat, which coincides with increased tectonic activity in the Baikal region at that time.

Thermobarometry of melts. To analyze basalts, we used liquidus thermobarometry by Albarede [26], which correlates with the thermobarometry by Ariskin [27]. The compositions were not saturated in olivine. It was supposed that the melt was fused out of a substratum reworked by earlier injection and metasomatism. The melts had mg# = (Mg/(Mg + Fe))~57–62%. Higher pressures and their scatter for picrobasalts are linked with contamination of peridotite material.

The magnesian basanites of the plateau base give a steep *PT* curve of intensive melting and upwelling (Fig. 4, *a*). The alkali-basalt magmas of the upper portion of the plateau continue this line. Hy-normalized lavas of the bottom correspond to the Moho discontinuity. The Pliocene-Pleistocene basanites and metahawaiites fall on

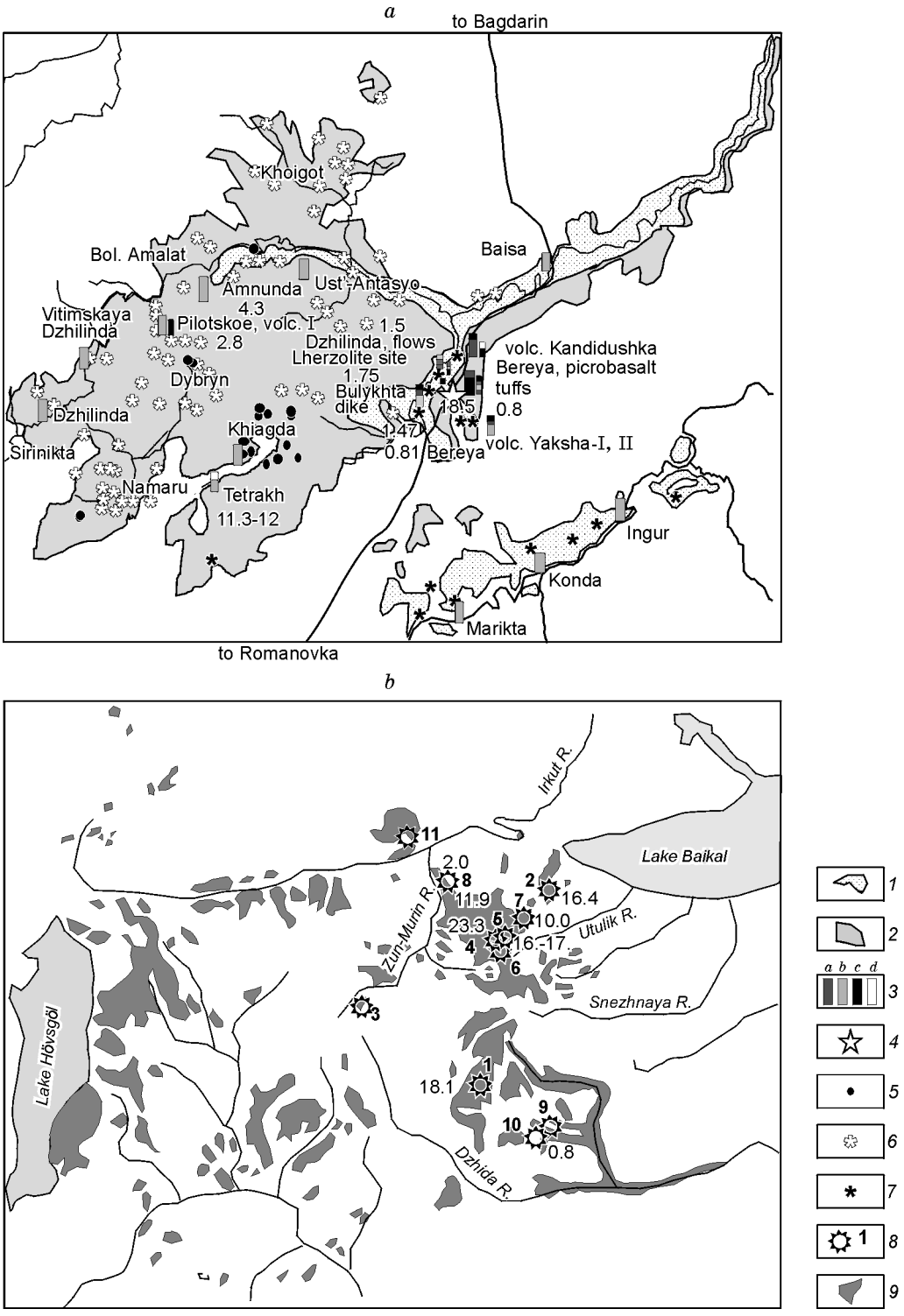

Fig. 2. Schematic structure of basalt plateaus: *a* — Vitim, *b* — Khamar-Daban. *1* — Pliocene post-erosional valley streams, *2* — Miocene basalt plateau, *3* — localities of mantle xenolith inclusions: *a* — garnet lherzolites, *b* — spinel lherzolites, *c* — pyroxenites, *d* — lower-crustal; *4* — Lower Miocene picrobasalt tuffs. Volcanoes: *5* — buried, *6* — Upper Miocene, *7* — Pleistocene; *8* — sites of xenolith sampling: 1 — Khubutui stream, 2 — Komar cover, 3 — Urunduchi volcano, 4 — Tumusun volcano, 5 — cover in lava thickness beneath Tumusun volcano, 6 — flow in basement of lava unit beneath Tumusun volcano, 7 — Margasanskaya Sopka volcano, 8 — flow in Margasan River opposite Marta River mouth, 9 — Bartoi volcanoes, 10 — volcanoes and covers of Tunka Valley (Khobok River, etc.); *9* — basalt fields. Numerals mean ages, Ma.

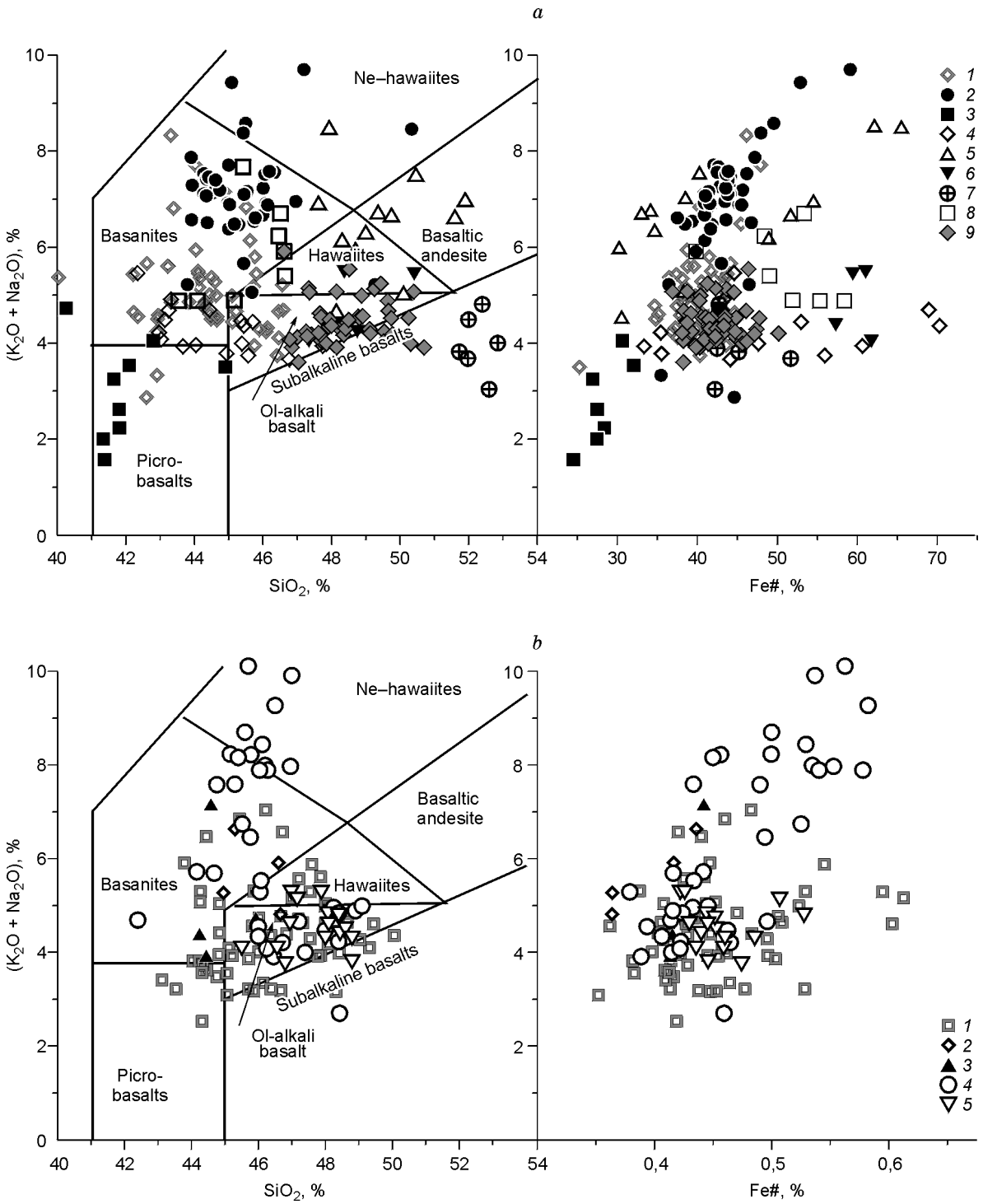

Fig. 3. Diagram SiO_2–Fe#–(K_2O + Na_2O) (TAS) for plateaus. ***a*** **— Vitim:** ***1*** **— Miocene Mg-basalts,** ***2*** **— Quaternary basanites and Ne-hawaiites,** ***3*** **— picrobasalts,** ***4*** **— low-potassium basanites,** ***5*** **— basaltic andesites,** ***6*** **— alkali ferrobasalts,** ***7*** **— subalkalic differentiated Hy-basalts,** ***8*** **— ferrobasanites,** ***9*** **— Miocene alkali flood basalts;** ***b*** **— Khamar-Daban:** ***1*** **— flood basalts (Miocene),** ***2***, ***3*** **— volcanic rocks of:** ***2*** **— upper part,** ***3*** **— basement,** ***4***, ***5*** **— basalts:** ***4*** **— Dzhida,** ***5*** **— Tunka.**

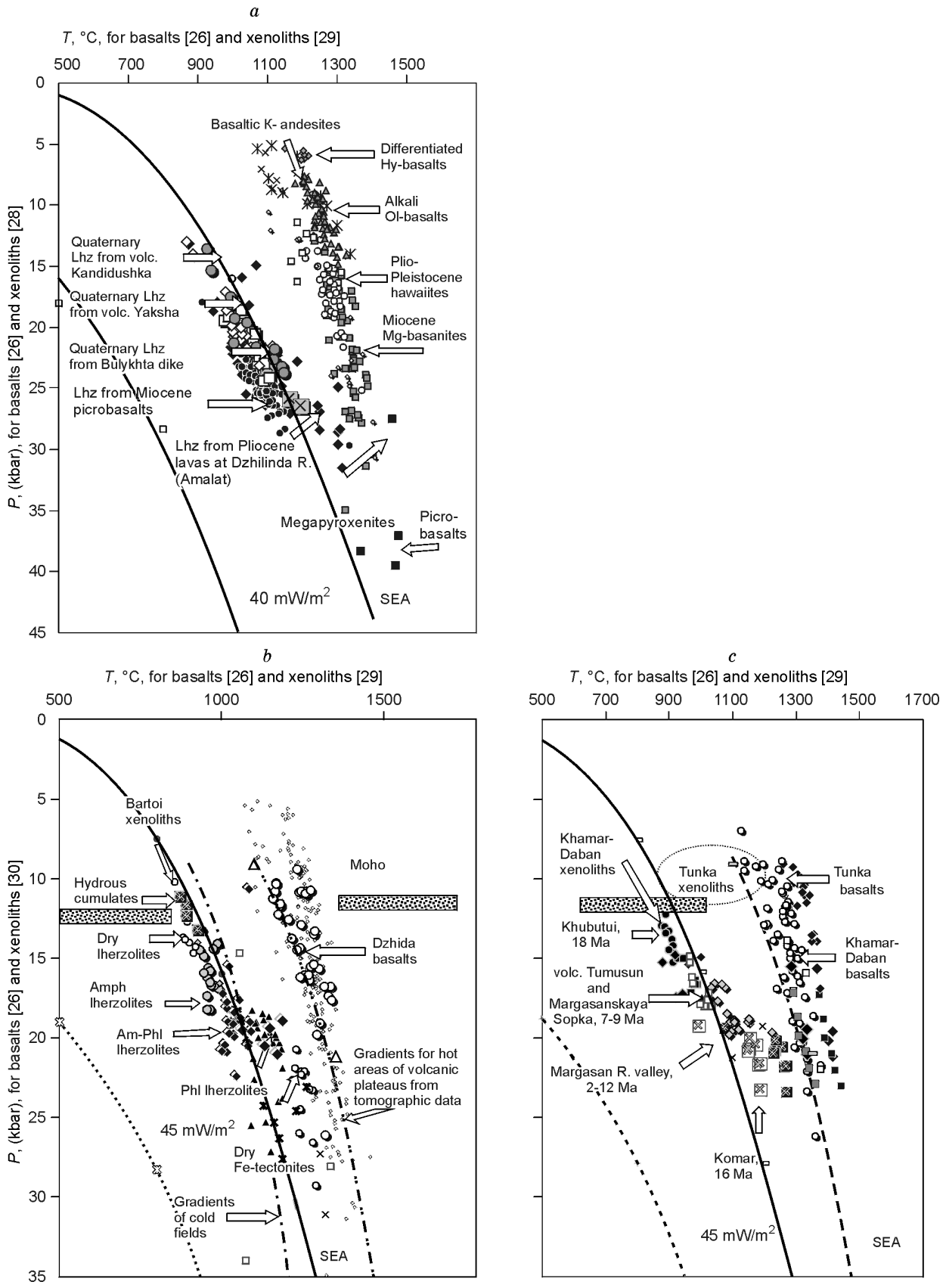

Fig. 4. Temperature regime in mantle of Vitim (*a*) and Khamar-Daban (*b*, *c*) plateaus from results of pyroxene [36, 37] (for xenoliths) and liquidus (for basalts) thermobarometry [26]. SEAG — Southeastern Australian geotherm [42].

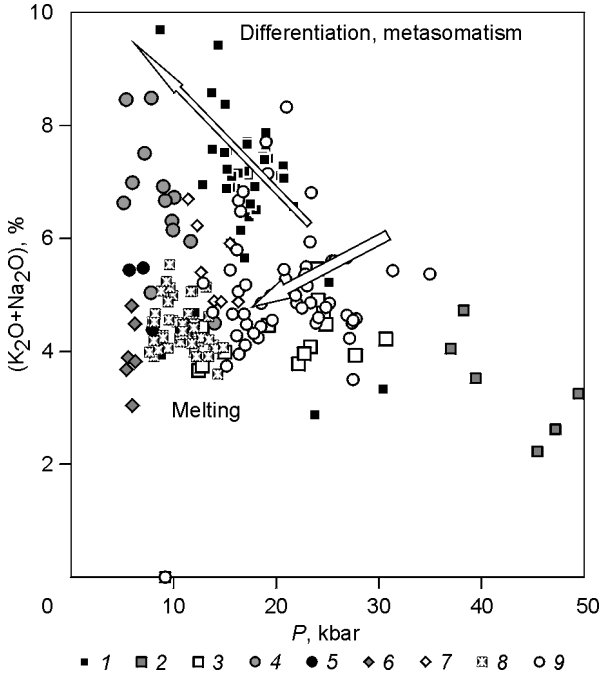

Fig. 5. Basalt alkalinity versus calculated depth of magma differentiation after [26] for basalts of Vitim plateau. *1* — Miocene Mg-basanites, *2* — Quaternary basanitoids and hawaiites, *3* — picrobasalts, *4* — low-potassium basanites, *5* — basaltic andesites, *6* — alkali Fe-basalts, *7* — differentiated Hy-basalts, *8* — Fe-basanites, *9* — Miocene alkali Ol-basalts.

the low-temperature branch in the garnet facies, which, along with a small volume of lavas, corresponds to the regime of stepwise upwelling with heat exchange and additional differentiation.

The Khamar-Daban basalts also demonstrate two branches of *PT* paths for hydrous and anhydrous melts [31] (see Fig. 4, *b*, *c*). The low-temperature branch (Dzhida basin, see Fig. 4, *b*) corresponds to basalts with amphiboles and micas in the bulk and/or in mantle inclusions, megacrysts, and the high-temperature one, to water-free melts. The Upper Miocene-Pliocene Tunka lavas as well as xenoliths are less high-temperature and less deep-seated, which is typical of permeable zones of rift valleys (see Fig. 4, *c*).

Two trends of chemistry of flood basalts reflect different modes of generation of magma melts (Fig. 5): the alkaline branch corresponds to accumulation of (Na_2O + K_2O) by assimilation of melt pockets and differentiation during the rise, and decreased alkalinity, to an increase in melting degree and jadeite component in the melting pyroxenes of peridotites.

At the Miocene-Pliocene boundary, when the major portion of lavas had been effused, the melts, migrating in the permeable lithosphere, formed local zones of magma generation at two levels in the mantle: near the boundary garnet facies and near the bottom of the crust. The Pleistocene cinder cones and flows are formed by melts from the top garnet facies.

Even within one block on the Vitim upland (headwaters of the Amnunda River), the regime of feeding (Fig. 6) varied, which is related to the tectonic regime, lithosphere permeability, and distance from the supplying plume jet.

Peridotite chemistry. There are four main chemical types of lherzolites [8]: 1 — primitive, close to the composition of primitive mantle [32, 33] (*P*-type); 2 — depleted, corresponding to restites of partial melting of *P*-lherzolites (*D*-type); 3 — Fe-lherzolites formed by interaction with ferriferrous basalt melts (*F*-type); 4 — enriched by the fractional crystallization of anatectic melt at the top of mantle sections represented by alumina-rich associations (*A*-type). The bulk compositions correlate with compositions of main rock-forming minerals, in particular, clinopyroxene. The *A*-type is characterized by low-iron Na-enriched pyroxenes, whereas the D-type has Na-poor Cr-enriched pyroxenes. The *F*-type contain >3% FeO for clinopyroxenes and elevated concentrations of TiO_2. The structural pattern of peridotites (Fig. 7) is related to the composition of peridotites: deformation structures are typical of the *F*-type; fine-grained structures of plastic flows, for the *A*-type; polygonal coarse-grained, of the *D*-type, and various protogranular, of the *P*-type.

Thermobarometry of inclusions. The uniqueness of the Vitim Plateau is that inclusions of the garnet facies

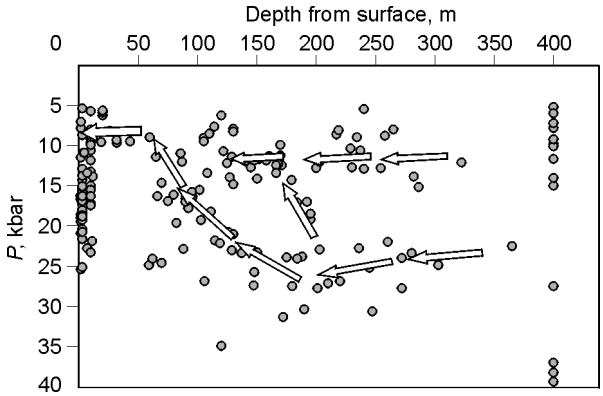

Fig. 6. Fluctuations of magma differentiation level defined after [26] as a function of depth of flow occurrence in lava in northern Vitim Plateau. Arrows show migration of magma generation centers by basalt plateau formation.

of the mantle are found in products of eruption of three stages of volcanic activity. Comparing geotherms for the Middle Miocene (Oligocene [8, 23]) and Pleistocene times, we estimated the heating at 50–100 °C [8, 34, 35]. The stage of Pliocene valley basalts is distinguished by diverse structures of mantle sections [35].

In addition to garnet-orthopyroxene barometry [28, 36], we used the orthopyroxene barometry [29, 37]. The correlation between these methods is more than 0.95 at $r \sim 0.94$. The check for xenoliths from volcanoes of the Hawaii islands [18], Malaita [38], Lesotho [39] showed a coincidence of *PT* diagrams. This method is appropriate for "primitive" compositions of lherzolites, whereas depleted peridotites and black pyroxenites give unreally high pressures, but the dynamics of temperature regime can be estimated. The slope of geotherms in the upper part of the spinel facies is conventional: Here, the Al_2O_3 isopleths for orthopyroxene are steeper [40]. However, in the mantle columns garnet relics occur even at $P < 15$ kbar, and orthopyroxene is often in equilibrium with it [8, 41].

The Vitim geotherms are subdivided into domains corresponding to rocks of a certain type and structural features (Fig. 8). Spinel peridotite, which are higher-temperature than garnets, form permeation paths on *PT* diagrams, which is in agreement with structural data and higher oxidation potential.

For the picrobasalt stage, the high-temperature branch corresponds to lherzolites with deformation structures and flow signs. The most of garnet lherzolites form a region with a steeper gradient than the conductive geotherm 90 mW/m^2 and even SEA [42] corresponds to decompression regime.

The most complicated *PT* diagram is that for xenoliths from the Pliocene valley lavas. Heating manifests itself in some stages of the mantle, including the top ones. The column beneath the Kandidushka volcano is characterized by permeable mantle with a high-temperature *PT* path. *PT* paths with a steeper slope than in SEAG (Southeastern Australia geotherm) [42], in the range 22–15 kbar, have been established for the Yaksha-I and Yaksha-II volcanoes, and for a dike near the source of the Bulykhta River.

Thus, it seems likely that the most part of the mantle sections are solidified or active mantle diapirs, with domains of permeation. They typically occur in the initial and especially in the final period of volcanic activity, when the mantle was drained by low-viscosity hydrous melts and veins and when interstitial microvein parageneses with amphibole and phlogopite were formed. Fe-Ti associations related to the filtration of alkaline melts also occur among the xenoliths of Pliocene stage but without hydrous minerals, which suggests essentially carbon-dioxide regime of formation of the most of lava.

In the trans-Khamar-Daban zone, a whole *PT* data set for xenoliths gives regularities close to the *PT* data for the Vitim xenoliths. The geotherm for xenoliths of the section base (Stage III) beneath the Tumusun volcano and in the Khubutui valley runs lower than SEAG [42]. The hot branch (Fig. 9, *b*) is formed by the xenoliths from the Komar Ridge (16 Ma). Inclusions of middle plateau horizons also belong to this stage (II) [8]. Inclusions of the Tumusun and Margasan volcanoes (III) provide continuous *PT* paths in the middle and upper parts of the spinel facies, which, as inferred from symplectites with garnet [8] and intergranular metasomatism [43], can be considered as a trend of the uplift of mantle diapir and melt migration. The posterosional stage (IV), recognized from xenoliths of the lavas at the Margasan River (opposite the Marta River mouth), is characterized by a layered section and reheating at the bottom of the column. The final stage (V) is represented by a complex of inclusions

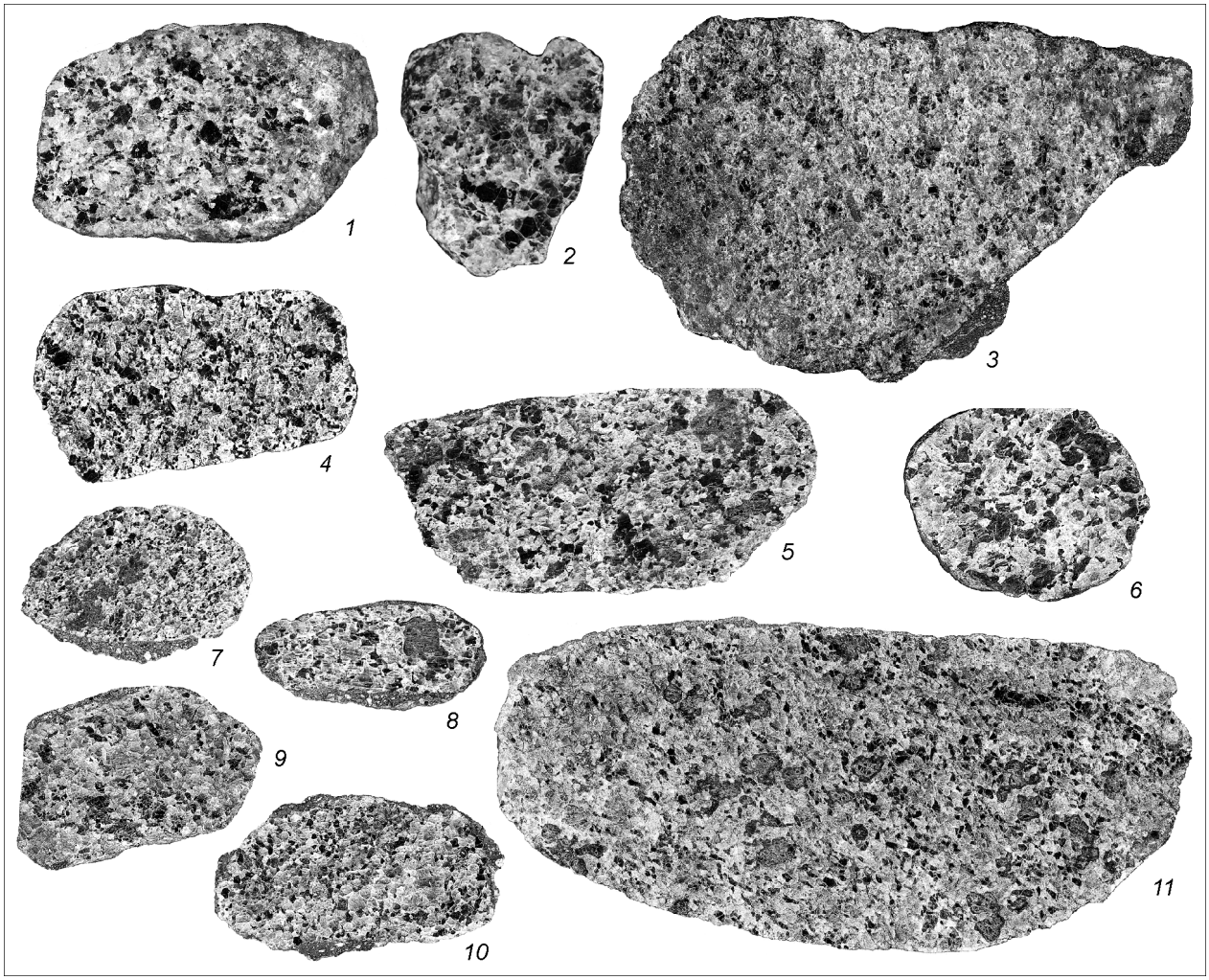

Fig. 7. Scanned images of various xenoliths of mantle lherzolites from picrobasalts and young volcanoes. Pleistocene Kandidushka volcano (Stage V): *1* — pseudogarnet lherzolite, *2* — spinel lherzolite, *3* — spinel websterite. Picrobasalt tuffs (Stage I): *4* — garnet lherzolite with ovoidal garnet and combination of structures of plastic flow and percolation, *5* — typical lherzolite with small-grained garnet, *6* — garnet lherzolite with dunite schlieren around garnet, *7* — lherzolite with alternating garnet and spinel zones with abundant clinopyroxene (of percolation), *8* — garnet peridotite with ovoidal garnet, rimmed by a light zone, *9* — Sp-lherzolite, *10* — Gr-Sp-lherzolite with melt percolation structure, *11* — Gr-lherzolite with fluidal structure and fold signs (size in large axis — 35 cm).

of the Bartoi volcanoes [8, 44], where the broken isotherms stand for Fe-lherzolites and phlogopite metasomatites, whereas the rest is close to SEAG [42].

DETAILED STRUCTURE OF MANTLE SECTIONS OF THE VITIM PLATEAU AT DIFFERENT STAGES

Mantle columns are reconstructed for three periods of volcanic activity of the Vitim Plateau. Peridotites are distinguished by a great diversity of structures (see Fig. 7) and composition. We used the method of temperature sections [38]: relationships T °C–Fe#(Na, Ti, Al, Cr) [8] for clinopyroxenes. The high-temperature trends of megacrysts follow the paths of rise and differentiation of basalt magmas at the initial stage of formation of magma conduits [45], and fine-grained pyroxenite inclusions are feathering veins. They form thickenings and clusters and regularly change the phase composition with temperature and depth from essentially clinopyroxene-garnet to plagioclase-clinopyroxene-amphibole ones, reflecting the evolution of the veined system during the rise of magma.

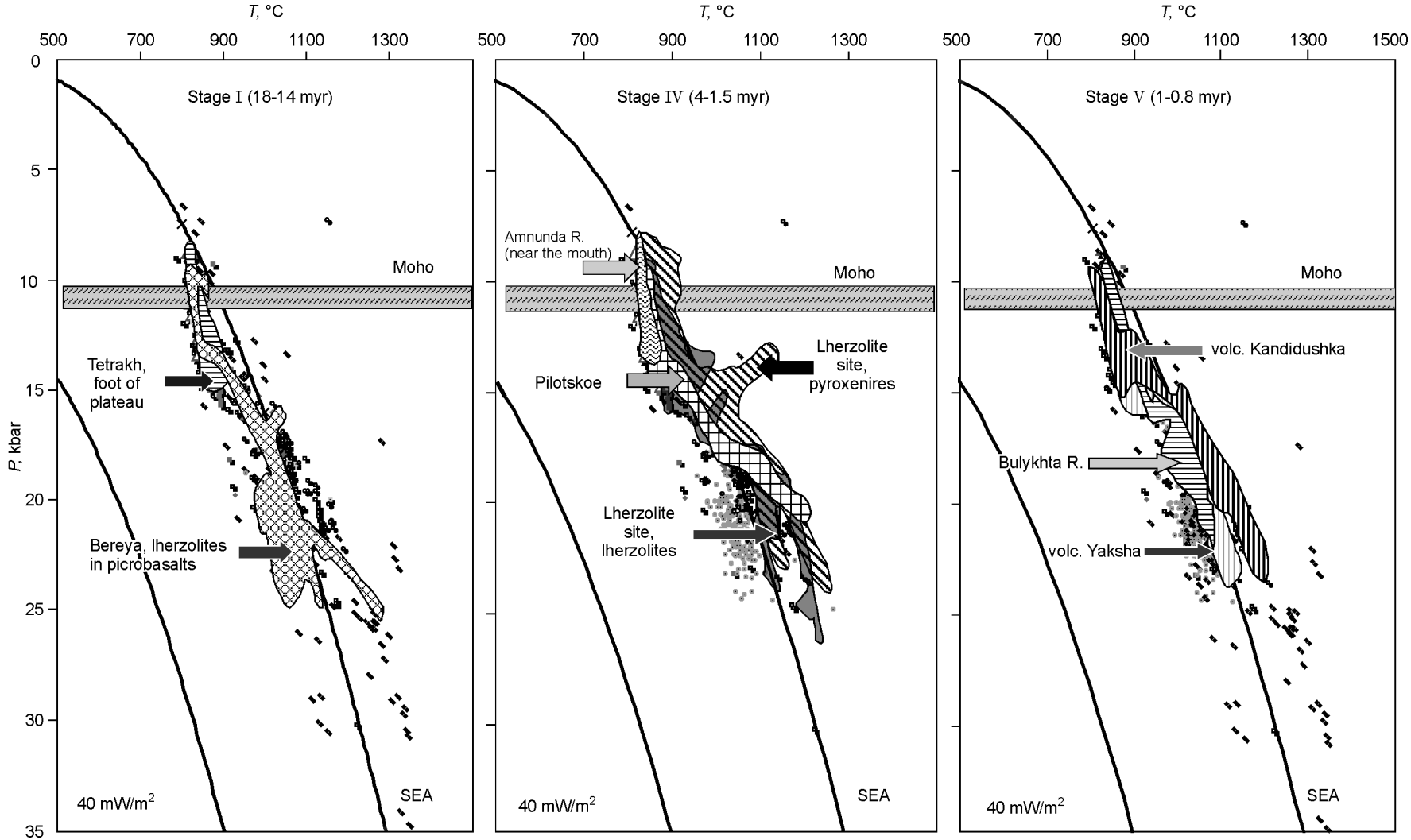

Fig. 8. Geothermal gradients for mantle below Vitim plateau determined by orthopyroxene thermobarometry from xenoliths (*P*, after [30]; *T*, after [36].

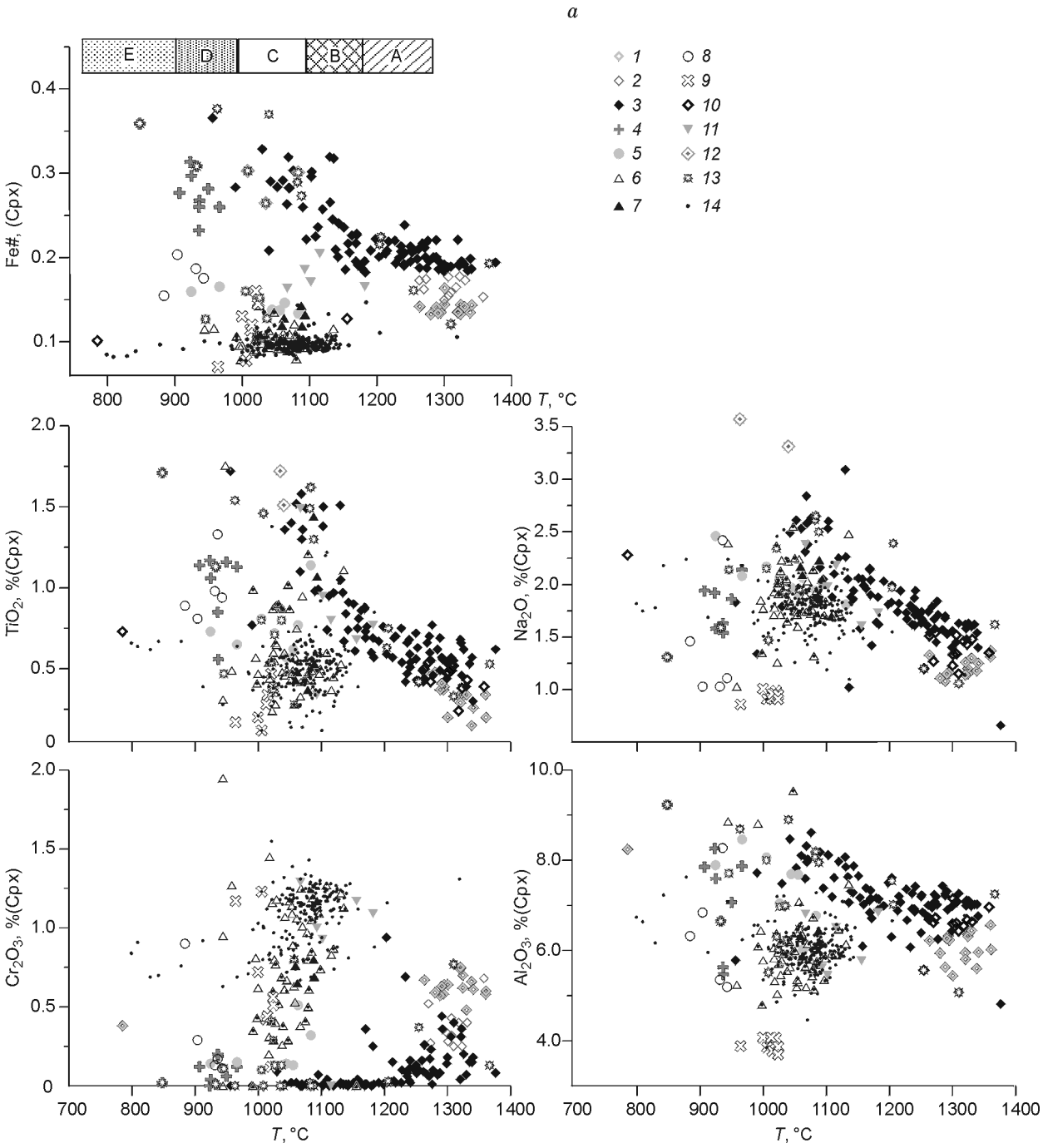

Fig. 9. Temperature sections (*T*, °C) — mineral composition for xenoliths from three stages of volcanism in Vitim Plateau. ***a*** **— for xenoliths from picrobasalts (Stage I): *1* — green high-temperature websterites; *2* — dark-green high-temperature websterites; *3* — black megapyroxenites; *4* — low-depth cumulates; *5* — hybrid low-temperature garnet-clinopyroxene veins; *6*, *7* — chrome-diopside websterites: *6* — anatectic, *7* — magmatic (hybrid); *8* — low-temperature hybrid websterites; *9* — low-alumina websterites; *10* — low-temperature spinel chrome websterites; *11* — high-temperature hybrid zonal phlogopite-kaersutite veins; *12* — black ilmenite megapyroxenite; *13* — samples analyzed on ICP MS; *14* — lherzolites.** ***b*** **— for xenoliths from posterosional streams (Stage IV) — "Lherzolite site": *1* — green high-temperature websterites; *2* — dark-green high-temperature websterites; *3* — hybrid high-temperature veins; *4* — anatectic Cr-diopside websterites; *5* — low-temperature basalt cumulates; *6* — low-temperature Fe-Ti-basalt cumulates; *7* — low-temperature melanocratic gneisses; *8* — low-temperature vein zonal basalt cumulates; *9* — "subsolidus" Cr-diopside websterites; *10* — black megapyroxenites; *11* — lherzolites.** ***c*** **— for xenoliths from cinder cones (Stage V): *1* — black megapyroxenites; *2* — garnet lherzolites; *3* — low-temperature spinel lherzolites; *4* — high-temperature spinel lherzolites; *5* — phlogopite lherzolites; *6* — Fe-lherzolites; *7* — Fe-Ti-lherzolites. For zones A–E see in text.**

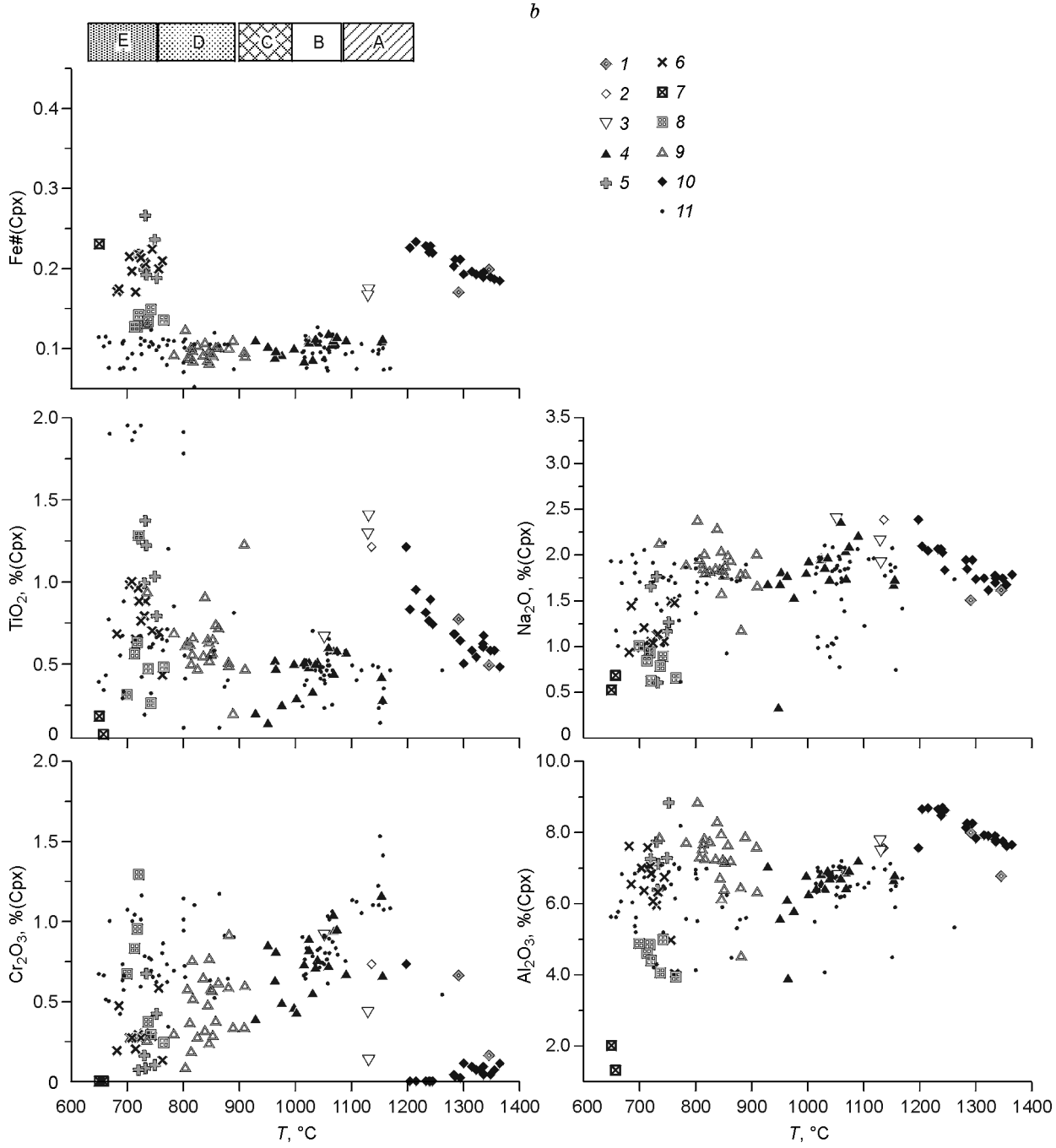

The multistage structure and change of veined parageneses and metasomatites seem to be related to the successive intrusion of melts to different levels and, possibly, on the contrary, to stop of the magma in hydrous horizons. Thermobarometry suggests the local character of manifestation of certain types of metasomatism and veined associations. Usually, temperature for peridotites and veined parageneses smoothly grows with depth, though some irregularity of heating is convincingly demonstrated by thermobarometry. Black pyroxenites are overheated by 50–150 °C relative to peridotites (see Fig. 8, *a*). No serious heat disturbances have been established for contacting pyroxenites and lherzolites, though sometimes the scatter of calculated pressures is 2 kbar, i.e. within an error.

On the basis of our own and literature [46–49] data (see Fig. 9, *a*) the following succession has been established for the *stage of Early Miocene picrobasalt tuffs* (I) [41, 47]. Zone (A) 1350—1250 °C—region of melt

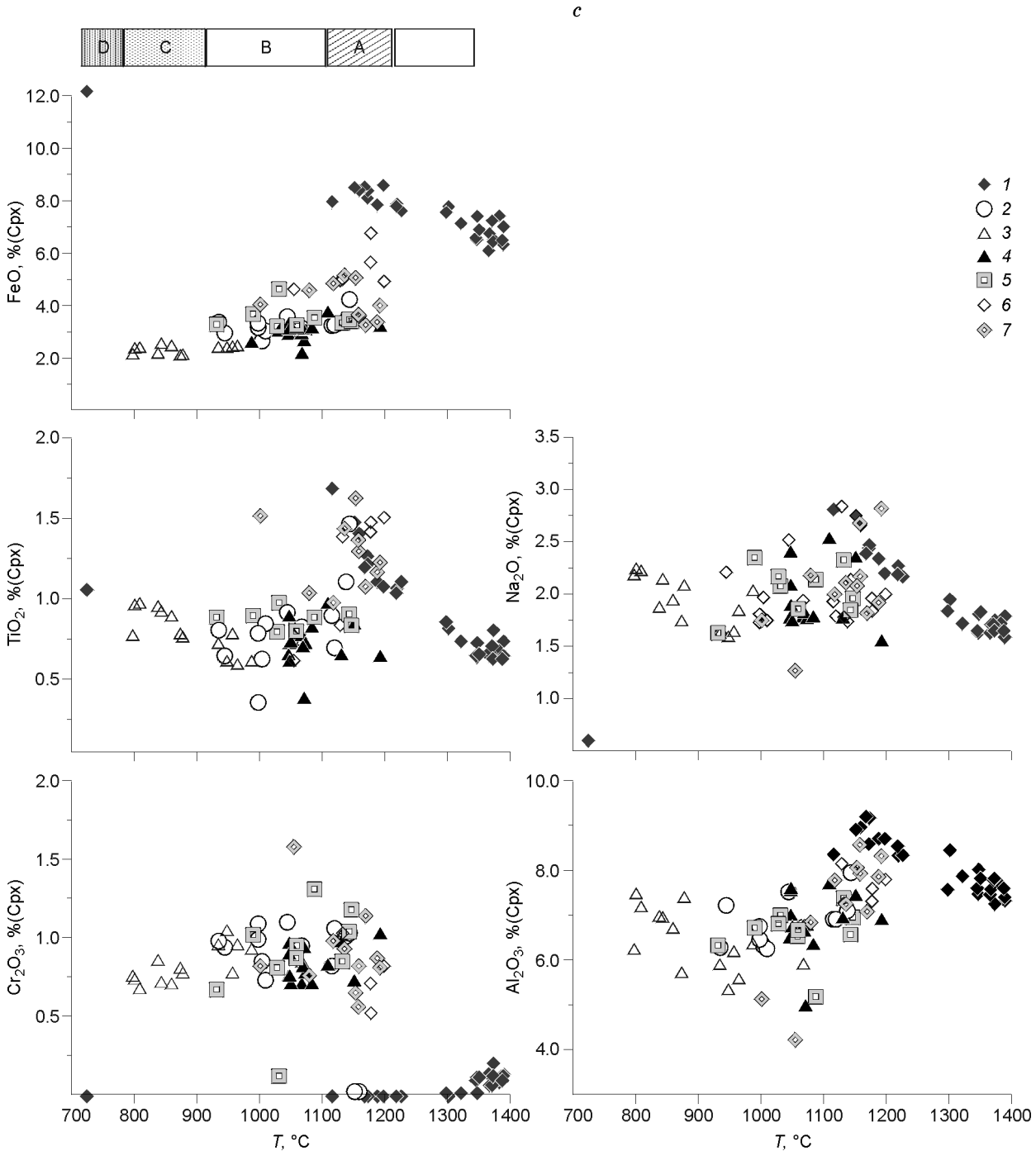

intrusion: black and green megapyroxenites, tectonized partly molten (about 1300 °C) garnet xenoliths [8, 34]; (B) — metasomatic and anatectic front: Fe-orthopyroxenites with kaersutite and ilmenite, Fe-Cr-diopside veins and rare comparatively high-temperature deformed peridotites; (C) — zone of plastic flow and penetration of melts: at the bottom — porphyritic garnet lherzolites with coarse garnet dunite clusters; (D) — more equigranular peridotite with alternating garnet and garnet-spinel zones, Cr-diopside pyroxenites, often Fe-enriched at the top of the interval, pargasite and phlogopite lherzolites; (E) — low-temperature branch: spinel lherzolites of *D-P* types; (F) — basalt cumulates at the Moho discontinuity.

Xenoliths from the bottom of the lava unit (II) of the Tetrakh valley permit reconstruction of the uppermost section with *D*- and *A*-type lherzolites.

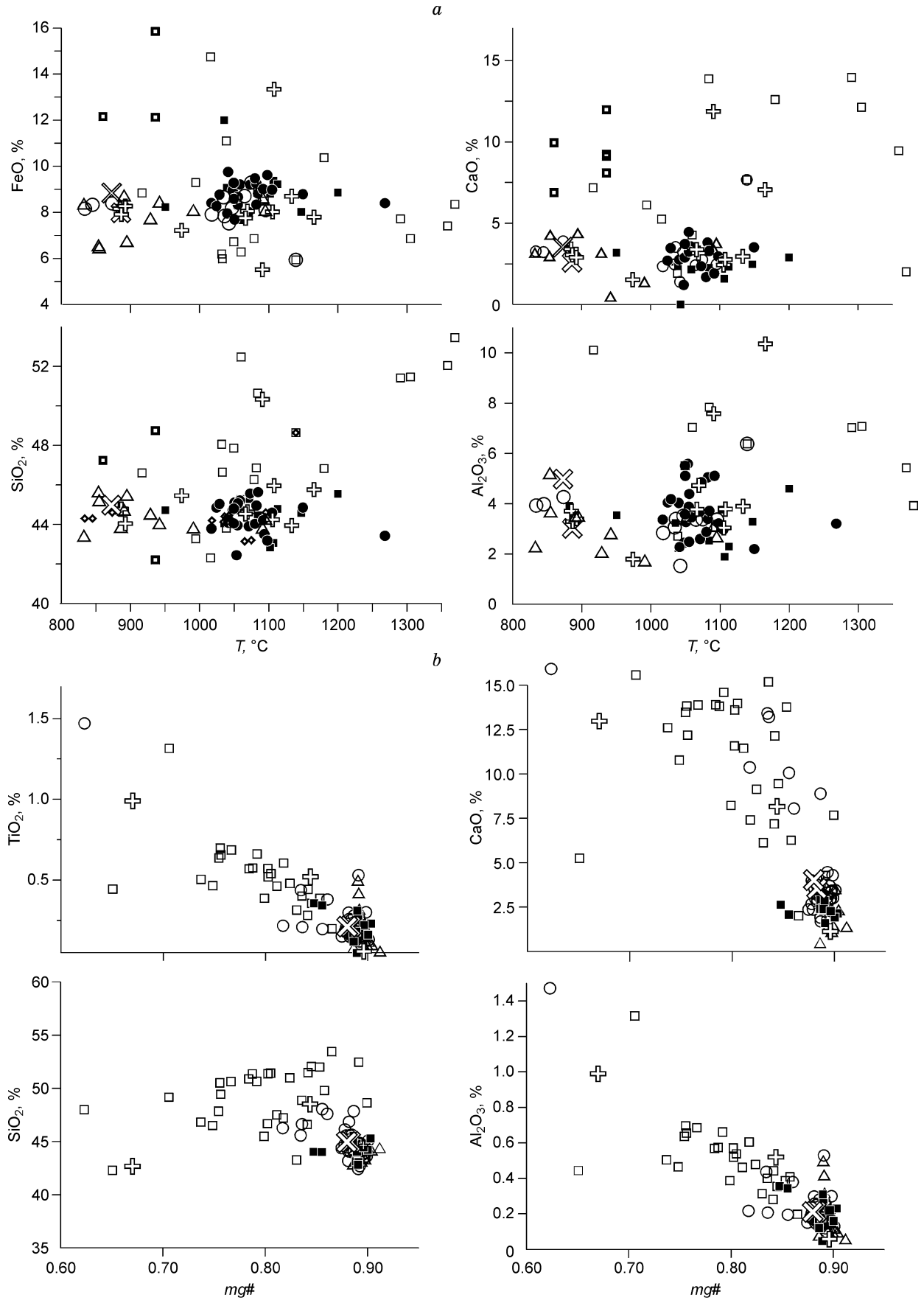
a
FeO, %
CaO, %
SiO2, %
Al2O3, %
T, °C
b
TiO2, %
CaO, %
SiO2, %
Al2O3, %
mg#

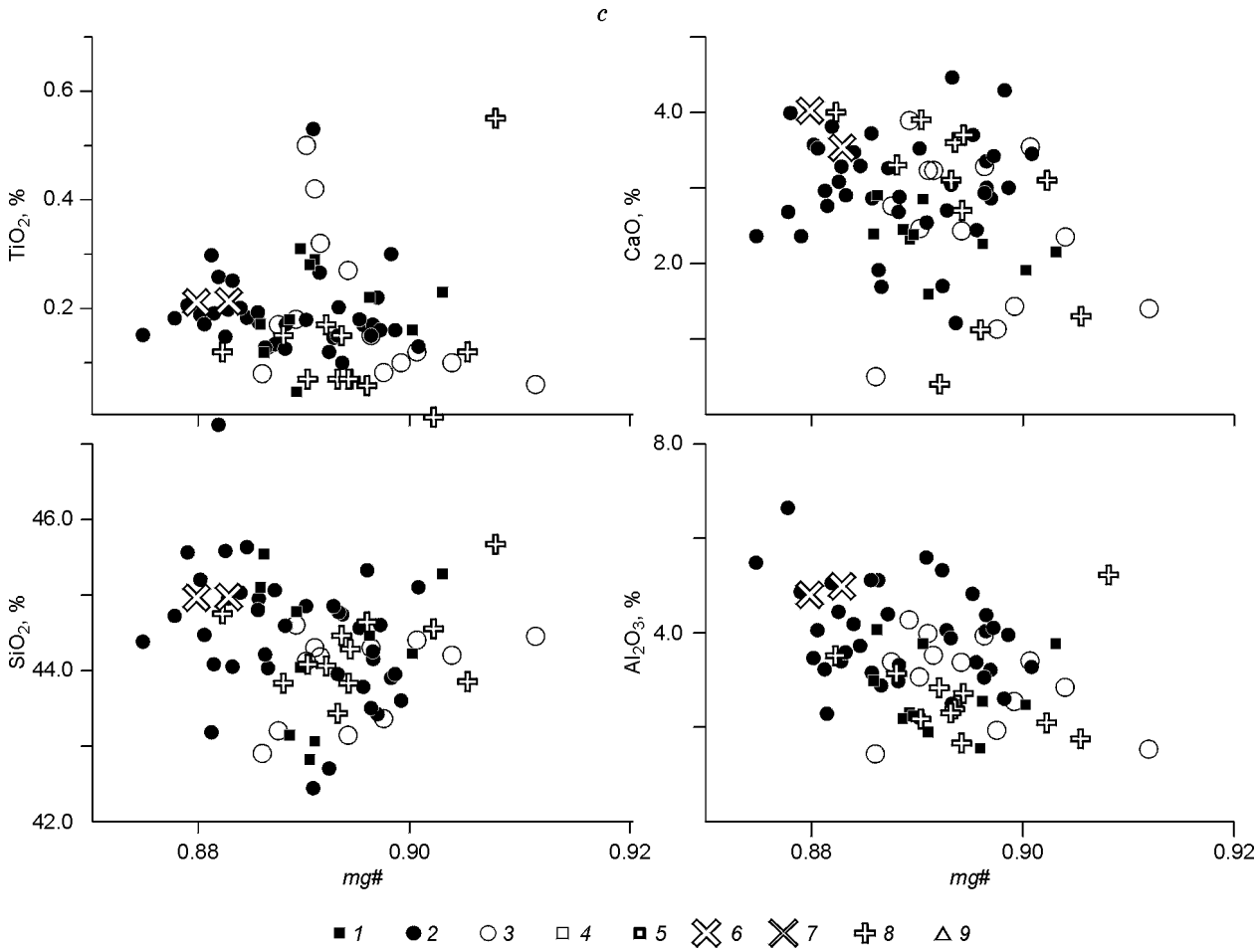

Fig. 10. Variation of bulk composition of peridotite and pyroxenite xenoliths as a function of: *a* — calculated temperature, after [36] (Opx), *b*, *c* — *mg*# = Fe/(Fe + Mg) a.u. Lherzolites: *1* — spinel, Kandidushka volcano; *2* — garnet from picrobasalts; *3* — spinel from picrobasalts; *4*, *5* — pyroxenites from picrobasalts: *4* — low-temperature, *5* — high-temperature; *6–9* — spinel lherzolites: *6* — Amnunda River (Stage III), *7* — Pilotskoe Lake, *8* — Dzhilinda River (Amalat), "Lherzolite site", *9* — Dzhilinda River (Amalat), other streams.

The Upper Miocene mantle section (III) reconstructed from xenoliths of the western volcano in the chain near Lake Pilotskoe has two zones: high-temperature (of *F*- and *P*-types) and low-temperature (*A*-type), typical of the final stage of the lava plateau formation when Na, Ti, and Al contents grow as temperature decreases.

The Pliocene section (IV) of the flow along the Dzhilinda River (Amalat lherzolite site) [35, 47, 50] is supplemented by data on the position of pyroxenites (see Fig. 9, *b*). There are pseudogarnet lherzolites ($T >$ 1240 °C) in zone A. Zone B is an asthenosphere jet (1180–1020 °C). It contains two horizons: of pseudo-garnet lherzolites and hybrid Fe-Ti pyroxenites (higher Zr/Y in Cpx). A horizon of Cr-diopside (hybrid) pyroxenites of zone B (1020–910 °C) separates it from zone E (910–800 °C) containing lherzolites of *F*- and *P*-types, Cr-diopside websterites of subsolidus type with garnet relics and exsolution lamelles, and Cr-diopside pyroxenites of magmatic habit. The low-temperature zone D (800–700 °C) contains *A*-, *P*-, and *D*-type lherzolites and pyroxenites of three levels of different iron enrichment.

On the basis of less abundant data, a similar section was reconstructed from xenoliths from the flow along the Dzhilinda River (Amalat), near the Kandidushka volcano.

The mantle section for the Kandidushka volcano of Pleistocene age (V) (see Fig. 9, *c*). Zone A of high-temperature interaction with basalt magmas (1200–1150 °C) contains Fe-pseudogarnet harzburgites and peridotites with various contents of Ti. Zone B, the asthenosphere jet (1150–950 °C), is composed of garnet lherzolites (of *P*- or *F*-type) with Fe-, Na-, and Cr-enriched pyroxenes. Zone C of decompression and rise of melts

(950–800 °C) contains diverse spinel *P*-, *F*-, and *A*-type lherzolites and is characterized by growing amounts of Na, Al, Fe, and Ti with a decrease in temperature. Zone D of crystallization (800–750 °C) is composed of basalt cumulates and rare *A*-type lherzolites.

For the Khamar-Daban xenoliths, the succession of mantle sections follows that for the Vitim Plateau, with the only exception that there are no peridotites of garnet facies and the mantle sections of different stages of volcanism are reconstructed for the deposits scattered over a large territory.

As for clinopyroxenes, **temperature-dependent rock composition** displays two trends: a decrease in contents of basaltoid components at $T > 900$ °C followed by a growth at crystallization of intergranular melts. Pyroxenites in the section change their composition in accordance with the mineralogy from high-temperature SiO_2-enriched websterites and clinopyroxenites to Al_2O_3-rich medium- and low-temperature black and green garnet (and even spinel) pyroxenites (Fig. 10, *b*). Taken together, the Khamar-Daban lherzolites of initial and intermediate stages give a trend of enrichment in Fe, Si, Ca, and Al with an increase in temperature, i.e., this is a progressive branch of regeneration. For the xenoliths of the Bartoi volcanoes, the trend of increased Si, Ca, Al, Na, and Ti with a decrease in temperature connotes the concentration of melts and crystallization (of pyroxenes) at the seepage front of melt percolation, i.e. this is a regressive branch.

GEOCHEMISTRY OF MINERALS OF MANTLE INCLUSIONS AND MELTS

Lherzolites. At the initial picrobasalt stage, the REE spectra for clinopyroxenes from lherzolites correspond to crystallization from melts formed during the modal melting of primitive lherzolites (Fig. 11). These are asymmetric arcuate spectra for the garnet facies, and nearly flat LREE-depleted spectra, for the spinel facies. Variations within a rock reflect the multistage evolution [51] of the composition of an interstitial film melt [52]. In minerals from amphibole lherzolites, the spectra are close to REE distributions of picrobasalt clinopyroxenes [46], suggesting the immediate filtration of plume melts through the lherzolite substratum [8, 32, 46] (see Fig. 11). The spectra of clinopyroxenes from high-temperature lherzolites with sheared structures are either close to basaltic [45, 46] or are flattened in the absence of flows and being out of equilibrium with nearly decomposed garnet (sp. 313-23). Cr-diopside pyroxenites form chiefly by melting of phlogopite metasomatites, whereas clinopyroxenites having spectra with HFSE peaks form by melting of amphibole metasomatites [49–52].

The spectra of clinopyroxenes of Stage III lherzolites correspond to the spinel facies spectra of enriched type without considerable extremums. For the stage of valley basalts (IV), the parental melts (according to coefficients of melt-pyroxene distribution) in the peridotites of the base of the mantle column (A) correspond to melting with a small share of garnet in the source. In the upper horizons (B–D) different degrees of melting (given recurrent passage of melts) and interaction of plume basalt melts with the lherzolite mantle are responsible for the diversity of spectra of rare elements of pyroxenes of lherzolites and pyroxenites. For the Cr-diopside series we can also suppose deep hybridization of a basalt melt with lherzolite substratum [51] rather than anatexis.

At the final stage (V) the Fe-lherzolites have the spectra similar to those of basalts. The peridotites of intermediate horizons have REE spectra corresponding to a small share of garnet and flat spectra, at the top of the spinel facies [47, 53] (see Fig. 11, Table 2).

Pyroxenites. The geochemistry of pyroxenite minerals was discussed in some papers [41, 45–53]. The clinopyroxenes from black pyroxenites have spectra of parental melts compositionally close to basalts but more differentiated, with a high La/Yb_n. The hybrid high-temperature varieties usually have a smaller dip of the wings because of the offset with flat-spectrum peridotite material. Low-temperature hybrid pyroxenites demonstrate "differentiated" REE spectra with high La/Sm_n and Gd/Yb_n, complicated by bends, often with maxima of high-field-strength elements that appear on melting of early pyroxenites and metasomatites.

The basalts from the explored volcanic plateaus are typical plume OIB melts (Fig. 12, Table 3). Their asymmetrical spectra form at 1% modal melting of primitive lherzolites of garnet facies [32]. The water-richest melts of the initial and final stages have elevated spectra with higher La/Yb_n and HFSE concentrations. These are Vitin picrobasalts and lavas of the Bartoi volcanoes. The typical flood basalts, in particular, magnesia basanites, have less enriched LREE spectra because of the intensive exchange with the peridotite (and pyroxenite) column.

DISCUSSION

Time evolution of chambers of magma generation. The Vitim Plateau is the most illustrative example of mantle evolution. During the period between eruptions, the composition of minerals (spinels and pyroxenes) changes nearly completely from garnet to spinel facies [8] (see Figs. 9, 11, 13). The mantle columns, at least near the magma conduit, seems to be nearly completely washed by melts. Peaks of Fe# on the plot *T* °C–Fe#Ol (see Fig. 13)

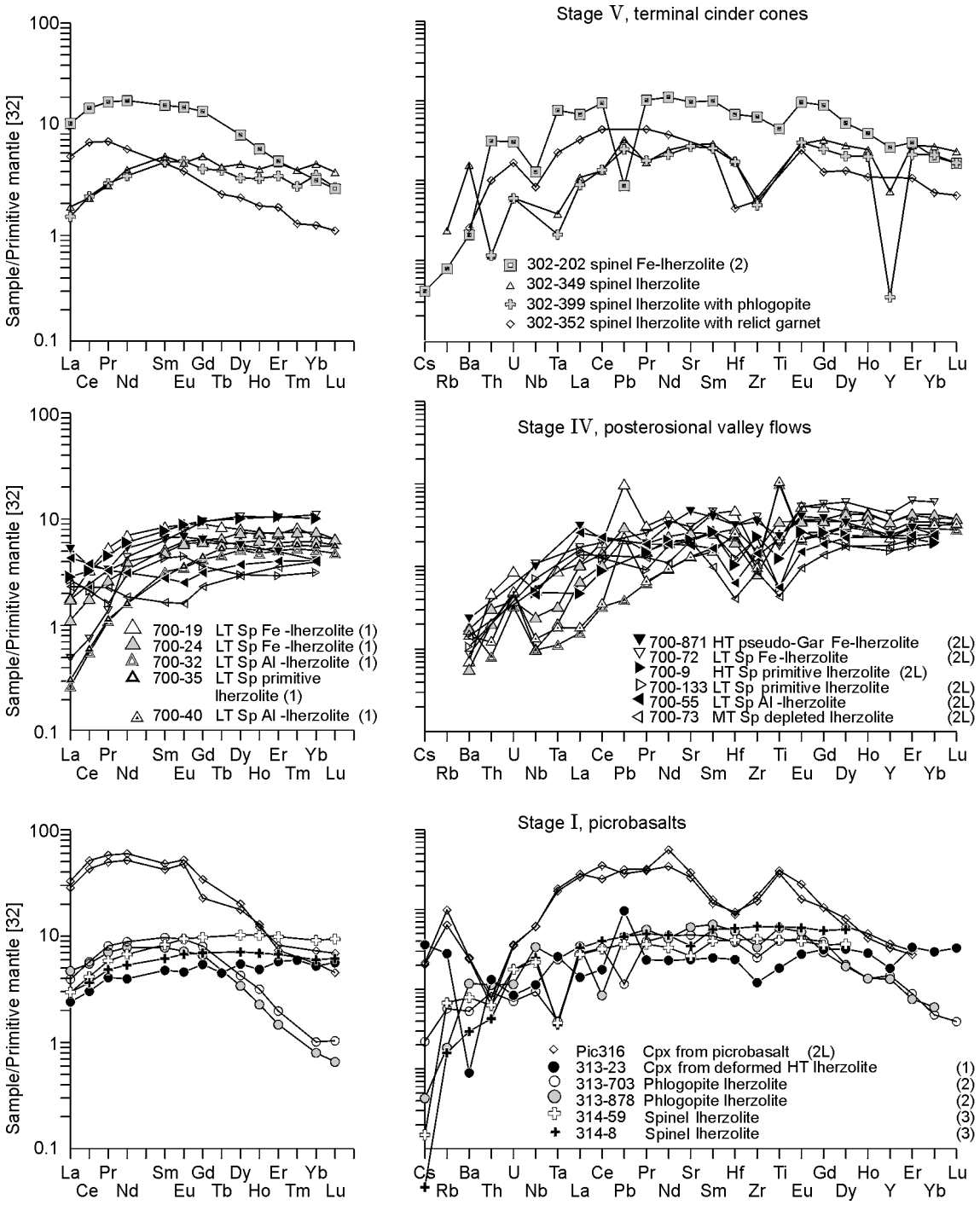

Fig. 11. Characteristic spectra of clinopyroxenes from lherzolite inclusions of three stages of volcanism development in Vitim Plateau. Numerals in parentheses: 1 — analyzed at Analytical Center of UIGGM SB RAN by ICP-MS with laser ablation, 2 — in laboratory of Royal Museum of Central Africa by chemical destruction, 2L — same place, by laser ablation, 3 — from [42].

must correspond to levels of concentration of basalt and hybrid melts. It is not clear to what extent xenoliths are indicative of changes in all domains of the mantle underlying the basalt plateau, but within the whole Bereya block the structure of mantle columns in the Pliocene is approximately the same over a distance of more than 20 km along the Dzhilinda River (Amalat) and in the south, in the Vitim valley, being absolutely different from

Table 2

Representative Analyses of Clinopyroxenes from Lherzolite Inclusions in Basalts of Vitim Plateau

Component	Stage I			Stage IV					Stage V
	313-23	313-703	313-878	700-19	700-24	700-32	700-35	700-40	302-202
	1	2	3	4	5	6	7	8	9
SiO_2	51.32	52.10	51.96	51.50	52.54	50.40	52.16	50.60	51.68
TiO_2	0.41	0.61	0.74	0.43	0.46	1.90	0.67	2.01	0.81
Al_2O_3	6.62	5.99	6.71	5.76	5.32	6.82	6.65	6.97	7.48
Cr_2O_3	1.31	1.14	0.99	0.51	0.54	1.00	0.59	1.10	0.91
FeO	4.18	3.47	3.81	3.58	4.47	2.09	2.93	2.16	4.07
MnO	0.10	0.81	0.08	0.06	0.11	0.04	0.11	0.05	0.10
MgO	17.94	15.52	15.80	14.66	18.87	14.07	14.24	14.21	14.90
CaO	15.21	18.16	16.76	22.78	16.42	21.25	21.31	20.60	16.32
Na_2O	1.28	1.61	2.37	1.03	0.77	1.95	1.85	1.91	2.58
Total	98.38	99.41	99.21	100.32	99.50	99.52	100.52	99.61	98.85
Ba	0.55	1.12	3.21	0.27	0.02				1.26
La	0.88	1.46	1.73	0.66	0.41	0.10	0.65	0.11	4.15
Ce	2.89	5.53	5.27	3.17	1.70	0.53	2.34	0.57	15.09
Pr	0.56	1.11	0.96	0.73	0.36	0.15	0.45	0.16	2.47
Nd	2.82	6.69	5.56	4.98	2.38	1.15	2.82	1.14	13.21
Eu	0.40	0.86	0.63	0.77	0.53	0.30	0.51	0.31	1.40
Sm	1.10	2.32	1.80	1.94	1.19	0.74	1.12	0.67	3.87
Gd	1.66	2.69	2.03	2.74	1.95	1.28	1.86	1.35	4.50
Tb	0.26			0.69	0.38	0.26	0.34	0.31	
Dy	2.08	1.86	1.30	3.05	2.82	1.95	2.29	2.01	3.36
Ho	0.41	0.28	0.19	0.64	0.62	0.40	0.53	0.43	0.56
Er	1.44	0.56	0.37	1.79	1.86	1.26	1.49	1.36	1.25
Tm	0.21	0.31	0.20	0.29	0.27	0.19	0.22	0.20	0.82
Yb	1.30	0.04	0.03	1.70	1.87	1.25	1.52	1.38	0.11
Lu	0.21	1.74	1.04	0.25	0.25	0.18	0.22	0.21	1.81
Hf	0.68			1.35	0.56	0.65	0.81	0.71	
Ta	0.09	0.12	0.01	0.03	0.01	0.00	0.01	0.01	0.27
Pb	1.74	0.15	0.20	1.78	0.39	0.07	0.54	0.40	0.15
Th	0.11	0.10	0.07	0.04	0.02	0.01	0.03	0.01	0.26
U	0.02	0.02	0.01	0.02	0.01	0.01	0.01	0.01	0.06
Au	0.02			0.02	0.01			0.02	
Co	26.91	24.50	17.64	16.41	17.00	14.09	14.75	12.91	16.39
Cu	56.31	6.83	3.72	257.16	23.64	4.48	24.66	27.76	2.46
Zn	7.42	17.04	8.10	151.43	35.28	29.67	19.20	48.01	13.42
Sr	48.49	78.90	87.20	53.28	43.33	27.22	52.90	26.68	176.00
Y	8.33	5.37	5.83	15.67	15.64	10.17	12.18	9.84	10.25
Zr	13.59	51.90	24.20	15.00	9.08	12.13	17.15	10.65	61.10
Nb	0.74	0.71	0.58	0.33	0.06	0.06	0.16	0.09	0.79
Rb		0.02	0.30						0.04
Cs		0.00	0.01						0.00
Sc		31.60	24.96						47.60
Ge		1.27	0.94						0.95
Mo		0.14	0.18						0.00
Analysis	(1)	(2)	(2)	(1)	(1)	(1)	(1)	(1)	(2)

Note. Analysis (1) is made at UIGGM SB RAS, Novosibirsk, by LAM ICP MS method (analysts A.I. Saprykin and P.A. Gerasimov); analysis (2) is made at Royal Museum of Central Africa by ICP MS method with chemical decomposition of monofractions.

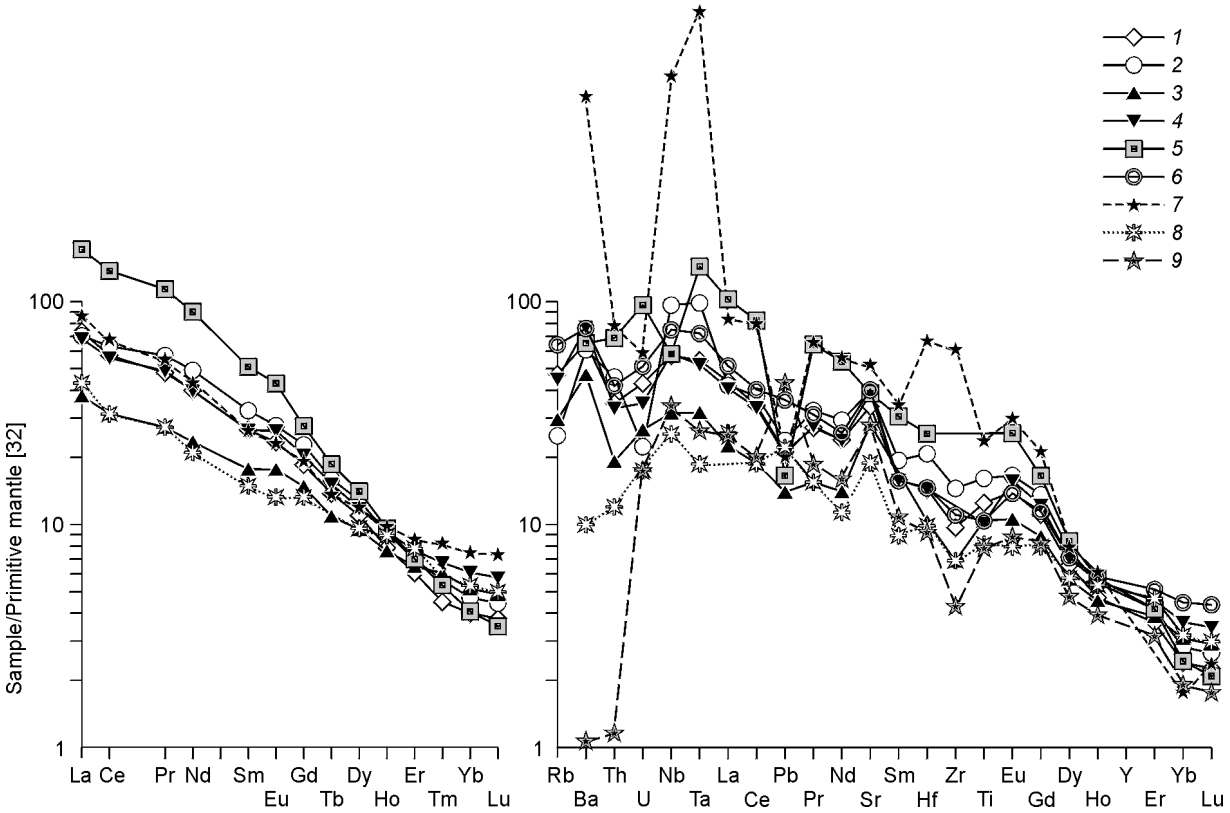

Fig. 12. REE characteristics of plume melts of Vitim Plateau and Khamar-Daban, after [9, 43, 47] and composition modeled melting of metasomatized mantle, pyroxenites, and lherzolites. Vitim Plateau: *1* — picrobasalt (Stage I), *2* — lavas with xenoliths from upper part of basalt plateau (Stage III), *3* — valley stream, *4* — Kandidushka volcano; Khamar-Daban: *5* — Bol'shoi (Bartoi) volcano, *6* — Tumusun volcano; model compositions: *7* — 1% melting of medium Vitim lherzolite, *8* — 5% melting of garnet olivine websterite, *9* — 1% melting of pargasite-phlogopite garnet lherzolite.

the mantle sections of the Pleistocene stage. The upper part of the spinel facies is close in chemistry of the II stage-lherzolites for the southern and northern groups of volcanoes. Veined pyroxenite systems in the mantle beneath each volcano are individual and seem to be developed locally, though chemically have much in common. In the most permeable blocks (Bereya), their structures are more variable laterally in sections of the mantle of the same stage. Each new pulse of volcanic activity erases the features of the preceding one, remelting the veined system and metasomatic associations and producing reaction changes. The bulk compositions of lherzolite and pyroxenite inclusions of garnet facies of picrobasalt stage (I) differ markedly from lherzolites of spinel facies in having a more primitive composition after [29] (see Fig. 12). Peridotites of Stage V are somewhat depleted, i.e., basalts seemed to remove a considerable share of alumina and calcium from the mantle (see Fig. 12). The abundance and diversity of anatectic and hybrid pyroxenites, which regularly change their composition upsection, being enriched in garnet (within the range 30–15 kbar), are drastically reduced in the Pleistocene time, but pyroxene-rich schlieren occur, which can form during the mechanical pull-apart of veins.

At the first stage the interaction with plume melts is traceable only from the spectra of rare elements in xenoliths with sheared structures [32]; the isotope composition of common garnet lherzolites [54] corresponds to DM (depleted mantle), though the amphibole-phlogopite veins and both black and green pyroxenites bear signs of plume magmas [45]. At the Pliocene stage the studied lherzolites are closer to OIB in isotopy, which is evidence of intensive mass exchange with basalt melts [46].

Within the trans-Khamar-Daban zone the mantle evolution has similar features. The thermal shock at the base of the spinel facies of the mantle (Stages I and II) expressed in high-temperature xenoliths of the Komar lava flow of Middle Miocene time caused melting with the formation of abundant green and hybrid pyroxenites. As inferred from the xenoliths of the Tumusun and Margasan volcanoes (Stage III), anatectic melts could percolate to form continuous *PT* trends and intense mantle diapirism could occur followed by the mechanical disintegration

Table 3

Representative Analyses of Basalts from Vitim Plateau and Khamar-Daban Ridge, after [43]

Element	Vitim Plateau					Khamar-Daban Ridge	
	Stage I	Stage II	Stage IV	Stage V		Stage III	Stage V
	Vi 87-1	Vi 402-1	371-2	Vi 302-36	302-17*	73-16	Vag8603-1
Ba	368	284	465	396	517	459	394
La	25.8	13.84	25	26.92	69.8	31.6	62.9
Ce	60.3	30.1	53.5	54.8	146.03	64.6	131.6
Pr	7.86	3.74	6.70	6.57	17.19	7.53	15.56
Nd	34.98	16.69	28.30	28.41	68.98	30.6	63.97
Eu	2.42	1.54	2.29	2.04	4.42	2.01	3.74
Sm	7.50	4.09	6.12	6.13	13.05	6.08	11.8
Gd	6.98	4.53	6.26	5.67	9.25	5.87	8.47
Tb	0.93	0.63	0.88	0.80	1.11	4.53	1.08
Dy	4.88	3.61	4.50	4.18	5.11	0.83	5.36
Ho	0.78	0.65	0.79	0.67	0.78	2.13	0.82
Er	1.73	1.61	1.90	1.51	1.76	1.85	1.74
Tm	0.20	0.22	0.24	0.16	0.21		0.19
Yb	1.16	1.28	1.51	0.99	1.04	0.28	1.01
Lu	0.17	0.19	0.22	0.14	0.12	4.18	0.13
Hf	5.94	2.96	4.13	4.13	4.47	2.53	7.32
Ta	3.46	1.12	1.83	1.91	3.19		5.05
Pb	4.18	2.45	3.60	3.70	5.11	3.41	2.90
Th	3.73	1.56	2.70	2.85	6.09	1.04	5.58
U	0.45	0.54	0.71	0.87	1.95	34.3	1.96
Rb	13.39	15.8	24	25.24	5.82	732	N.d.
Sr	722	513	705	617	1957	N.d.	»
Y	Not determined					187	»
Zr	246	116	198	164	57.23	46.2	»
Nb	59.6	19.5	36.00	35.36	209	N.d.	»
Cs	Not determined				0.49	0.79	»

*** Analysis is carried out at Analytical Center of UIGGM by LAM ICP MS method, analyst A.I. Saprykin.**

of diverse veins and relative homogenization of the mantle column [8]. Supposedly, the layered sections reconstructed by xenoliths from flows along the Margasan River (Stage IV) correspond to the overbedding of percolation waves and/or mantle diapirs. Still more differentiated mantle section formed by a complicated process of differentiation and splitting of rising basaltoid melts with polybaric zones of percolation is typical of the Bartoi volcanoes (Stage V) in the southern Khamar-Daban (Table 4) and other regions of Transbaikalia [55].

In some cases, the heterogeneities may be supposed to be due to intrusion of rising melts percolating through peridotites, and a group of monotypic xenoliths may be considered a horizon, but for the known mantle sections the bedding is more typical.

Basalt genesis. The Sr-Nd isotope data for the Vitim basalts [9] suggest a primitive (radiogenic) source for picrobasalts (Bulk Earth). The isotopically close lavas of Pleistocene age are more alkaline [47]. The Pliocene basanites and Ne-melahawaiites are admixed with lherzolite material. The magnesian basalts from the plateau are still more contaminated. Simulation of the assimilation of the peridotite bulk composition yields an unreally high

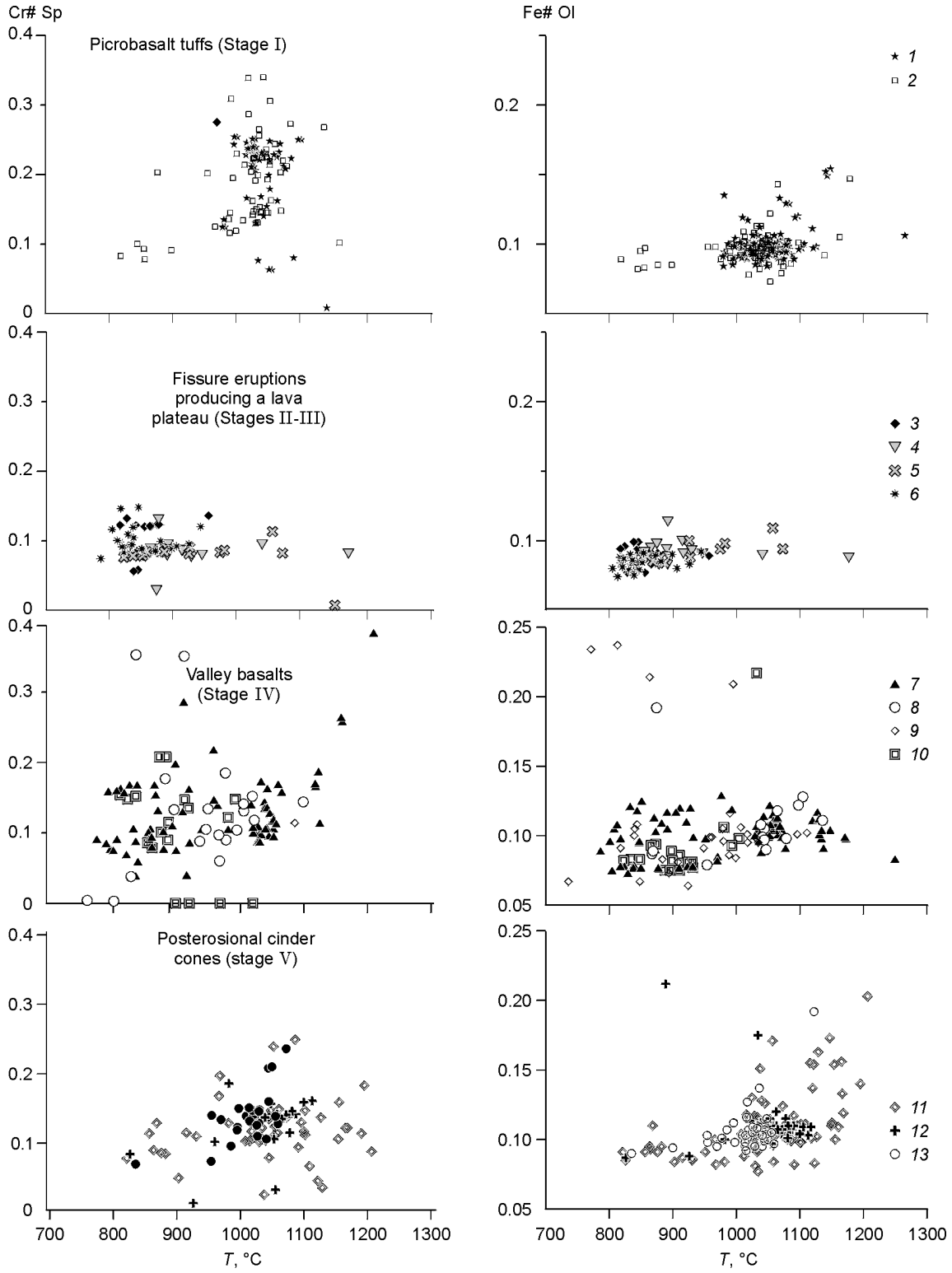

Fig. 13. Variations of Fe#Ol (Fe/(Fe + Mg) a.u.) and Cr#Sp (Cr/(Cr + Al) a.u.) versus temperature after [36] for some stages of Vitim Plateau development. Lherzolites from picrobasalts: *1* — garnet, *2* — spinel, *3* — Tetrakh River, lower reaches, *4* — Amnunda River, upper part of plateau, *5* — volcano I near Pilotskoe Lake, *6* — Dzhilinda River (Vitim). Flows along Dzhilinda River (Amalat): *7* — "Lherzolite site", *8* — 3 km downstream from "Lherzolite site", *9* — near Kandidushka volcano, *10* — flows along Vitim River, *11* — Kandidushka Volcano, *12* — Yaksha volcano, *13* — dike,

share of the contaminant. During the assimilation of the most fusible component, clinopyroxene, its share must be about 95% if its isotopy corresponds to the MORB type, and about 70%, if it corresponds to the DM type. During the assimilation crystallization of AFC ($R \sim 0.9$), the amount of the reacted DM-type material is more than 35%. This mechanism explains the change in composition of peridotite minerals and variations in basalt compositions with depth. Taking into account that clinopyroxene, a concentrator of REE and Sr, amounts to 10–15% in rock and that usually its isotopy changes in the aureole of a magmatic system, the share of the reacted peridotites must be 10–50 times as great as the volume of basalts. Some part of the melt remains in the mantle and lower crust in the form of pyroxenites, and this amount may be enlarged by an order of magnitude. With a thickness of basalt covers of 200–500 m the basalt-altered peridotite column of the same size must be no less than 50–250 km. The domain of magma generation has extended roots, and plume melts flow down in permeable zones [16, 17, 56] from deep-seated sources [57].

The behavior of rising melts is regulated by volumes and mode of migration of the volatiles dissolved in a melt at high degrees of melting during the plateau formation and migrating to the initial and final stages to form melt pockets [18]. The drop in K_2O content in the Miocene basanites and alkaline basalts of Vitim (see Fig. 5) is governed by an increase in melting degree (from about one to 2.5% and more) and by a decrease in the share of metasomatic components or melting packages [18], which occur in the Vitim lherzolite inclusions [8]. Correlation of the obtained pressures with Na_2O (see Fig. 6) for the Miocene basanites corresponds to the equilibrium with peridotite (in which jadeite end-member in clinopyroxene grows with depth) and agree with the regime of gradual migration of melts. In the posterosional basanite-hawaiites the share of Na_2O and K_2O grows with a decrease in pressure by remelting of pyroxenite metasomatites from the upper parts of the mantle columns, assimilation of melting packages [18], and additional differentiation. The similarity of geochemical REE characteristics of basalts within the Vitim Plateau [9] implies a homogeneous source of melting. Using the average data on the bulk composition of the Vitim Plateau [29], we have established that the Stage V lavas of the Kandidushka volcano can be obtained by 0.9% melting, whereas the preceding valley basalts (Stage II) have somewhat greater degree of melting at a smaller portion of garnet. Fe-lherzolites are also appropriate (sp. 302-202) [45]. Judging by Nb-Ta maxima, picrobasalts imply the participation of amphibole (kaersutite). Flood basalts with a comparatively flat distribution of REE form by melting of olivine websterites (~1.5% garnet and ~30% olivine). To compensate the LILE and HFSE deficiency, the presence of a fluid, amphibole, and phlogopite is necessary. The Khamar-Daban basalts of the Tumusun volcano (Stage III) also must have no less than 2–3% garnet in the melting association (in its absence from xenoliths). The Bartoi lavas with a higher La/Yb_n suggest a degree of melting of about 0.8%, no less 10% garnet in restite, and the contribution of metasomatic minerals at about 3–5%. The initial basalt melts there and at other deposits melt out at a greater depth than the depth of xenolith entrapment, which is in agreement with high temperatures of liquidus thermobarometry for basalts and "hot" pyroxenites, about 1350 °C. The intersection of a lherzolite and a basalt *PT* paths yields about 50–60 kbar. This also coincides with estimates for depths of melting of oceanic basalts [58]. Interaction proceeds at the upper horizons. During the formation of a basalt plateau, the arriving melts follow not only the easiest path, through pyroxenites and metasomatized lherzolites, but also the path through the olivine matrix, changing completely the characteristics of minerals of mantle peridotites. The "hot" converted peridotites and pyroxenites from the domain of magma generation are rarely brought to the surface, being dissolved in basalt melts owing to the composition similarity. As seen from Fe# maxima at temperature sections, the melts usually rise step by step to form polybaric systems. The existence of vast zones of melting within 20–30 kbar is due to a minimum at the peridotite solidus in the presence of volatiles [59].

The basalt plateaus of Central Asia are localized in a segment focusing two descending convective branches of submerged plates off Indostan and western Pacific. The mechanism of generation of lava plateaus as a result of separation of volatiles and melting with the participation of eclogite plates [60] in the domains with a heated mantle is probable near the continental margin. The appearance of alkaline flood basalts is typical at the rear of the Mediterranian subduction zones (from Central Massif to Pannonia [61]), North America and South America (Patagonia) [62]. The source of plume basalts is, probably, the same [61], localized at the boundary with the core, and variations in the basalt geochemistry [63] are controlled by the upper stories of the mantle. The effect of the submerged plate on the mantle plume at the upper-lower mantle boundary at a rate of subduction of 2–3 cm/year will have a sensible effect in 30–50 myr at a distance of about 500 km. To reach the core, the time must be longer, but the range of effect will be much wider.

Starting with the Pacific margin, the basalt plateaus are 500–600 km apart from one another [4], which can be controlled by a size of isometric convection cells above the excited lower mantle. The subduction funnel at the joint of two descending convective branches must provide material for melting and appearance, on rising, of vast domains of concentration at the phase-transition boundaries, where the inversion of melt density occurs in the

Table 4

Stages of Volcanism and Mantle Columns beneath Volcanic Plateaus

Stage of basalt plateau development	Time boundaries, Ma*	Relief	Volcanism: lava composition and eruption types	Mantle xenoliths of lherzolites	Pyroxenites	Metasomatism	Mantle column structure
I — initial prerift	18 – 14 22 – 20	Gentle uplifts and depressions	Picrobasalts, Hy-normalized lavas and leucobasalts in some depressions	Garnet lherzolites with gradual change of structure from coarse- to fine-grained with changing mineral composition	High-temperature polyphase pegmatoid of black series, pegmatoid hybrid (or of picrite melts), various high- and low-temperature veins	Hydrous scattered phlogopite in depth in garnet facies, microveined phlogopite and pargasite in upper part of garnet and in spinel (pargasite) facies	Polybaric chambers but one basic melting zone
II — formation of basement of lava plateau	14 – 10 18 – 17	Filling of valleys and beginning of rise	Flood Mg-basalts and alkali basalts	Medium- and fine-grain Sp-lherzolites with Al-enriched minerals	Hybrid high-temperature, essentially orthopyroxene	Nondisplayed or high-temperature (1200 C), ferriferous	Uniform in upper part of section of basalt-tested spinel facies, cumulates in basement of crust
III — lava unit	9 – 5 17 – 9(7)	Levelling of relief and plateau formation	Flood alkali and subalkali basalt lavas	Sp-lherzolites of Al-type, structures of percolation and decompression (symplectites to garnets), slight Fe- and Ti-enrichment of low horizons	Black high-temperature, Cr-diopside of hybrid type	Fe-Ti medium-temperature (1000–1100 C), anhydrous in lower part of spinel facies	Two-member: upper part — lherzolite section of Al-type, lower part — primitive moderate-Fe
IV — initial posterosional	2 – 1.3 7 – 2	Insets (~20–50 m) of river network to flood basalts	Alkali basalts with glomeroporphyrous twins, extrusions of basanites and cinder cones sticked in lava plateau	In lower part of mantle — pseudogarnet lherzolites; higher — spinel lherzolites arising on melting filtration, decompression of previous pulses of plume activity, upper horizon — collectors of basalt melts in spinel lherzolites, low-temperature Al-enriched lherzolites	Various anhydrous, black pegmatoids, Cr-diopside hybrid, subsolidus and black cumulative lherzolites in basement of crust	Fe-Ti around local polybaric magma chambers hidden	Layered at expense of localization pf levels of infiltration and superposition of some pulses of plume activity during lava plateau formation
V — final posterosional	1 – 0.8 1.5 – 0.8	Canyons incised in central part of plateau	Valley cinder cones in depressions and rift valleys on lava plateau periphery	Fe- and Ti-enriched lower horizons — lherzolites, higher — decompressed spinel with relics of garnet, upper — Na-enriched Al-spinel lherzolites	Cr-diopside percolation and hybrid. Black fine-grained in Vitim, in Bartoi— various, often hydrous	Fe-Ti-high-temperature. Phlogopite in garnet-clinopyroxene veinlets in garnet-spinel transition level. In Bartoi — various in all levels	Layered, with three-member section. Lower part is high-temperature, enriched, basalt-aletered, medium — zone of filtration and unwarping of diapirs, upper — relict with Al parageneses

*** Above line — for Vitim Plateau; below line — for Khamar-Daban Ridge.**

peridotite mantle (660, 410 km), caused by second-order plumes [4, 64], spreading along the roof of the lithosphere. The appearance of a magma at the top is controlled by the lithosphere structure, i.e. the presence of melt-permeable tectonic zones and fusible metasomatites and pyroxenites, which usually trace the boundaries of plates or large tectonic blocks.

The productivity of the oceanic plateaus of the Hawaiian and Azores types [21] and other hot spots is 2–3 orders of magnitude higher than any of the Central Asian spots (~10^{-4} km^3/year for the Vitim Plateau). As a rule, hot spots have the roots extending to the core [16], whereas the roots of wide domains of diffused continental basalt magmatism are not so deep-seated [62, 65].

CONCLUSIONS

Basalt volcanism and mantle sections bear features of rapid and joint evolution. The regularities are close for two explored districts. The differences are related mainly to the intensity of volcanism and amount of melt in the mantle, which depends on the total permeability of the structure, considerably exceeding that for the trans-Khamar-Daban zone, where the intense mantle diapirism is expressed, probably, promoting the growth of orogens. There is a correlation between the relief and plume position [66]. The geotherms of mantle peridotite central parts of folded structure are hotter than the geotherms of the periphery. Beneath the orogens, in zones of plume magmatism, the amount of melts may be rather high, and the mantle diapirs support them from beneath. Only the great thickness of the crust does not permit the melts to effuse immediately, so they effuse along the periphery of slopes through radial fractures (see Figs. 1 and 2, *b*). A general scheme of mantle evolution during the formation of lava plateaus is shown in Table 1.

The appearance of low-viscosity interstitial melts, which is usually expressed in the presence of vitreous films on the grains, was a possible cause of the formation and rise of the asthenosphere over a large area of the Baikal region in the Pliocene-Pleistocene. Along with tectonic deformations, this might be responsible for the intense rifting at the final stage. Percolation of such melts along the boundaries of the lithosphere broken on extension might account for the cellular structure of convection, when the low-viscosity melts envelop denser and colder blocks [67, 68].

In general, the development of lava plateau resembles a scheme of development of large shield volcanoes [69] and is controlled by the melt rise dynamics, leading to the growth of uplifts, and by the collapse of deep-seated reservoirs in the process of depletion with the cave-in of the domal structure.

To conclude, we state that:

1. The volcanic plateaus within the Baikal Rift Zone formed during the Miocene-Pleistocene had diachronous initial and coeval final pulses of magmatism.

2. There are five periods of volcanic activity recognized on the Miocene-Pleistocene volcanic plateaus within the Baikal region, which are marked by the appearance of xenolith-bearing basalts.

3. The final stage of the appearance of low-viscosity deep-seated melts with high K/Na on the Vitim Plateau, Khamar-Daban, and Udokan is linked with the total rise of the asthenosphere within the BRZ, lower viscosity, and more active tectonic regime.

4. Mantle sections quickly change in areas with active volcanism and, though having much in common in chemistry, at some stages close volcanoes show nonuniform heating and composition of mantle columns owing to individual character of processes that occur in the roots of deep-seated volcanic systems.

5. Joint evolution of mantle matter, basalt volcanism and tectonic relief-forming processes is similar for many areas of the Baikal region and other zones of plume volcanism, including the oceanic plateaus.

We thank all colleagues participating in laboratory and field works: S.V. Kanakin, M.A. Kalmanovich, S.V. Esin, N.F. Krasov, V.G. Mal'kovets, K.D. Litasov, Yu.D. Litasov, A. Tugolesova, A.A. Golovin, et al. We also thank the reviewers, V.N. Sharapov and S.V. Rasskazov, for constructive criticism.

This work was supported by grants 94-05-1710003 and 99-05-65688 from the Russian Foundation for Basic Research and by the grant of UIGGM on the project "Petrology of upper mantle of rift zones".

REFERENCES

1. Martynov, Yu.A., and S. Okamura, Isotopic ratios of strontium in high-alumina basalts of Eastern Sikhote-Alin': application to the geodynamic regime under which the Sea pf Japan formed and opened, *Dokl. RAN*, **362**, 1, 94–97, 1998.

2. Korago, E.A., and A.N. Evdokimov, Post-Miocene continental alkali-basalt volcanism of northern Eurasia, *Petrologiya*, **7**, 1, 80–98, 1999.

3. Smith, A.D., The geodynamic significance of the DUPAL anomaly in Asia, in M.F.J. Flower (Ed.), *Mantle dynamics and plate interactions in East Asia*, 89–106, AGU, Washington, 1998.

4. Semenova, V.G., L.V. Solov'eva, and B.M. Vladimirov, *Mantle-derived inclusions in alkali basaltoids of Tokinsky Stanovik* [in Russian], 117 pp., Nauka, Novosibirsk, 1984.

5. Rasskazov, S.V., *Udokan basaltoids* [in Russian], 142 pp., Nauka, Novosibirsk, 1985.

6. Stupak, F.M., *Cenozoic volcanism of Udokan Ridge* [in Russian], 169 pp., Nauka, Novosibisrk, 1987.

7. Kiselev, A.I. M.E. Medvedev, and G.A. Golovko, *Volcanism of Baikal Rift Zone and problems of mantle-derived magma formation* [in Russian], 197 pp., Nauka, Novosibirsk, 1979.

8. Ashchepkov, I.V., *Mantle-derived xenoliths of Baikal Rift* [in Russian], 160 pp., Nauka, Novosibirsk, 1991.

9. Esin, S.V., I.V. Ashchepkov, V.A. Ponomarchuk, and M. Yamamoto, *Petrogenesis of alkaline basaltoids from the Vitim plateau: Baikal rift zone*, 58 p., UIGGM SB RAS, Novosibirsk, 1995 (Prepr. No. 2, UIGGM SB RAS).

10. Grachev, A.F., Khamar-Daban — hot spot of the Baikal Rift according to data of chemical geodynamics, *Fizika Zemli*, **3**, 3–28, 1998.

11. Rasskazov, S.V., *Magmatism of the Baikal rift system* [in Russian], 286 pp., Nauka, Novosibirsk, 1993.

12. Kurgan'kov, P.P., *Geodynamic setting of Cenozoic volcanism of Tuva and problem of intracontinental rifting. PhD Thesis* [in Russian], 460 pp., IZK SO RAN, Irkutsk, 1998.

13. Yarmolyuk, V.V., V.I. Kovalenko, V.P. Kovach, S.V. Budnikov, I.K. Kozakov, A.B. Kotov, and E.B. Sal'nikova, Nd-isotope systematics of crustal magmatic protoliths of Western Transbaikalia and problem of Riphean crust formation in Central Asia, *Geotektonika*, 4, 3–20, 1999.

14. Zonenshain, L.P., M.I. Kuzmin, and N.Yu. Bocharova, Hot field tectonics, *Tectonophysics*, **199**, 165–192, 1999.

15. Windley, B.F., and M.B. Alen, Mongolian plateau: evidence for a Late Cenozoic mantle under central Asia, *Geology*, **21**, 295–298, 1993.

16. Bijwaard, H., and W. Spakman, Tomographic evidence for a narrow whole mantle plume below Iceland, *Earth Planet. Sci. Lett.*, **166**, issue 3–4, 121–126, 1999.

17. Ebinger, C.J., and N.H. Sleep, Cenozoic magmatism throughout East Africa resulting from impact of a single plume, *Nature*, **395**, 788–791, 1998.

18. Sen, G., A. Macfarline, and N. Srimal, Significance of rare hydrous melts in Hawaiian xenoliths, *Contrib. Miner. Petrol.*, **122**, 415–427, 1996.

19. Zhang, M., P. Suddaby, R.N. Thompson, M.F. Thirwall, and M. Menzis, Potassic volcanic rocks in NE China: geochemical constraints on mantle source and magma genesis, *J. Petrol.*, **36**, 5, 1275–1303, 1995.

20. Rasskazov, S.V., A.V. Ivanov, I.S. Brandt, S.B. Brandt, and S.B. Lomyga, Magmatism development at weakened rifting, in *Results of detailed study of Late Cenozoic Bereya volcanic range in Vitim Upland* [in Russian], 56–58, IZK SO RAN, Irkutsk, 1996.

21. Rasskazov, S.V., N.A. Logachev, I.S. Brandt, and A.V. Ivanov, *Geochronology and geodynamics of Late Cenozoic (South Siberia—South and East Asia)* [in Russian], 300 pp., Nauka, Novosibisrk, 2001.

22. White, R.S., and D.M. McKenzie, Mantle plume and flood basalts, *J. Geophys. Res.*, **100**, 17,543–17,585, 1995.

23. Ashchepkov, I.V., N.L. Dobretsov, and M.A. Kalmanovich, Garnet peridotites from alkali picritoids and basanitoids of Vitim Upland, *Dokl. AN SSSR*, **302**, 2, 417–420, 1998.

24. Rasskazov, S.V., M.J. Kunk, J.F. Luhr, S.A. Bowring, I.S. Brandt, S.B. Brandt, and A.V. Ivanov, Episodes of eruptions and compositionsl variations of the Quaternary lavas in the Baikal Rift System (Ar-Ar and K-Ar dating of volcanism in the Dzhida River area), *Geologiya i Geofizika (Russian Geology and Geophysics)*, **37**, 6, 3–15(1–12), 1996.

25. Rasskazov, S.V., A.V. Ivanov, I.S. Brandt, and S.B. Brandt, Migration of Late Cenozoic volcanism of Udokan field in structures of Baikal and Olekma-Stanovoi systems, *Dokl. RAN*, **360**, 3, 378–382, 1998.

26. Albarede, F., How deep do common basaltic magmas form and differentiate, *J. Geophys. Res.*, **97**, 10,997–11,009, 1992.

27. Ariskin, A.A., Phase equilibria modeling in igneous petrology: use of COMAGMAT model for simulating fractionation of ferro-basaltic magmas and the genesis of high-alumina basalt, *J. Volcanol. Geotherm. Res.*, **90**, 1–2, 115–162, 1999.

28. Nickel, K.G., and D.H. Green, Empirical geothermobarometry for garnet peridotites and implication for the nature of lithosphere, kimberlites and diamonds, *Earth Planet. Sci. Lett.*, **73**, 158–170, 1985.

29. Bertrand, P., and J.C.-C. Mercier, The mutual solubility of coexisting ortho- and clinopyroxene: toward the absolute geothermometer for the natural system?, *Earth Planet. Sci. Lett.*, **76**, 122–152, 1985.

30. Perkins, D., and R.C. Newton, The compositions of coexisting pyroxenes and garnet in the system $CaO–MgO–Al_2O_3–SiO_2$ at 900–1100 °C and high pressures, *Contrib. Miner. Petrol.*, **75**, 291–300, 1980.

31. Flower, M.F.J., K. Tanaki, and N. Hoang, Mantle extrusion: a model for dispersed volcanism and DUPAL like asthenosphere in east Asia and the western Pacific, in M.F.J. Flower (Ed.), *Mantle dynamics and plate interactions in East Asia*, 67–88, AGU, Washington, 1985.

32. McDonough, W.F., and S.S. Sun, The Composition of the Earth, *Chem. Geol.*, **120**, 3–4, 223–253, 1995.

33. Jagoutz, E., H. Palme, H. Baddenhausen, et al., The abundance of major, minor, and trace elements in the Earth's mantle as derived from primitive ultramafic nodules, in *Proc. Lunar. Planet. Sci. Conf.*, 2031–2050, 1979.

34. Dobretsov, N.L., and I.V. Ashchepkov, Melt migration and depletion - regeneration processes in upper mantle of continental and ocean rift zones, in T. Peters et al. (eds.), Dordrecht/Boston/London, Kluwer Academic Publishers, *Ophiolite Genesis and Evolution of oceanic Lithosphere*, 125–147, 1991.

35. Ashchepkov, I.V., L. Andre, V.G. Malkovets, and K.D. Litasov, Stratification of upper mantle columns beneath Vitim plateau in Miocene and Quaternary, in *Absr. 6th Int. Kimberlite Conf.*, 20–22, Novosibirsk, 1995.

36. Brey, G.P., and T. Kohler, Geothermobarometry in four phase lherzolites II: new thermobarometers and practical assessment of using thermobarometers, *J. Petrol.*, **31**, 1353–1378, 1990.

37. McGregor, I.D., The system $MgO–SiO_2–Al_2O_3$: solubility of Al_2O_3 in enstatite for spinel and garnet peridotite compositions, *Amer. Miner.*, **59**, 110–119, 1974.

38. Nixon, P.H., and F.R Boyd, Garnet-bearing lherzolites and discrete nodule suites from the Malaita alnoite, Solomon Islands, S.W. Pacific, and their bearing on oceanic mantle composition and geotherm, in F.R. Boyd, H.O.A. Meyer (eds.), *The mantle sample inclusions in kimberlite and other volcanics*, 400–423, AGU, Washington, 1979.

39. Nixon, P.H. (Ed.), *Lesotho kimberlites*, 305 pp., Cape and Transvaal Printers Ltd., Cape Town, 1973.

40. Gasparik, T., Orthopyroxene barometry in simple and complex systems, *Contrib. Miner. Petrol.*, **96**, 3, 357–370, 1986.

41. Ashchepkov, I.V., L. Andre, V.G. Malkovets, Yu.D. Litasov, and A.V. Travin, The Stages of the Melt Percolation in the Mantle Beneath Vitim (Transbaikal), *J. Conf. Abstr.*, **4**, 1, 362, 1999.

42. O'Reilly, S.Y., and W.L. Griffin, A xenolith-derived geotherm for southeastern Australia and its geological implications, *Tectonophysics*, **111**, 41–63, 1985.

43. Ionov, D.A., S.Y. O'Reilly, and I.V. Ashchepkov, Feldspar-bearing lherzolite xenoliths in alkali basalts from Hamar-Daban, Southern Baikal region, Russia, *Contrib. Miner. Petrol.*, **122**, 1–2, 174–190, 1995.

44. Melyakhovetsky, A.A., I.V. Ashchepkov, and N.L. Dobretsov, Amphibole- and phlogopite-bearing mantle xenoliths and related inclusions of Bartoi volcanoes (Baikal Rift Zone), *Dokl. AN SSSR*, **286**, 5, 1215–1219, 1985.

45. Ashchepkov, I.V., and L. Andre, Pyroxenite xenoliths in picrite basalts (Vitim Plateau): origin and differentiation of mantle melts, *Geologiya i Geofizika (Russian Geology and Geophysisc)*, **43**, 4, 343–363(328–347), 2002.

46. Glaser, S.M., S.F. Foley, and D. Gunther, Trace element compositions of minerals in garnet and spinel peridotite xenoliths from the Vitim volcanic field, Transbaikalia, eastern Siberia, *Lithos*, **48**, 263–285, 1999.

47. Ashchepkov, I.V., A.V. Travin, L. Andre, and O.S. Khmelnikova, Cenozoic flood basalt magmatism: Mantle xenoliths and melting regions in the lithospheric mantle of the Baikal rift and other regions of Central Asia, in *Alkaline magmatism and the problems of mantle sources*, 161–176, Institute of Geochemistry, SB RAS, Irkutsk, 2000.

48. Ionov, D.A., I.V. Ashchepkov, H.-G. Stosch, G. Witt-Eickschen, and H.A. Seck, Garnet peridotite xenoliths from the Vitim volcanic field, Baikal region: the nature of the garnet-spinel peridotite transition zone in the continental mantle, *J. Petrol.*, **34**, 6, 108–125, 1993.

49. Ionov, D.A., and A.W. Hofmann, Nb-Ta-rich mantle amphiboles and micas: implications for subduction-related metasomatic trace element fractionations, *Earth Planet. Sci. Lett.*, **131**, 341–356, 1995.

50. Ashchepkov, I.V., and L. Andre, Cr-Diopside Veins in Vitim Mantle. Origin and evolution, *J. Conf. Abstr.*, **4**, 1, 358–359, 1999.

51. Ashchepkov, I.V., V.J.R. Salters, and L. Andre, Relationships between garnet and clinopyroxene in Vitim mantle xenoliths: evidence of the polystage growth and melt percolation?, in *Seventh International Kimberlite Conference. Cape Town. Extended Abstracts*, 35–36, 1998.

52. Andre, L., and I.V. Ahschepkov, Acid leaching experiments on the mantle-derived Vitim clinopyroxenes: implications for the role of the clinopyroxenes in the mantle processes, in D. Demaiffe (Ed.), *Petrology and Geochemistry of magmatic suites of rocks in the continental and oceanic crusts. A volume dedicated to Professor Jean Michot*, 321–336, Universite Libre de Bruxelles, Royal Museum for Central Africa (Tervuren), 1996.

53. Litasov, K.D., S.F. Foley, and Yu.D. Litasov, Magmatic modification and metasomatism of the subcontinental mantle beneath the Vitim volcanic field, East Siberia: evidence from trace element data on pyroxenite and peridotite xenoliths from Miocene picrobasalt, *Lithos*, **54**, 83–114, 2000.

54. Ionov, D.A., and E. Jagoutz, Sr and Nd isotope composition of garnet and spinel peridotite xenoliths of Vitim Upland: first data for mantle inclusions of the USSR, *Dokl. AN SSSR*, **301**, 5, 232–236, 1988.

55. Ashchepkov, I.V., Yu.D. Litasov, and K.D. Litasov, Xenoliths of garnet lherzolites from metanephelinites, the Khentei Ridge (Southern Transbaikalia): evidence for the uplift of mantle diapir, *Geologiya i Geofizika (Russian Geology and Geophysics)*, **37**, 1, 130–147(121–137), 1996.

56. Davies, G., A channelled plume under Africa, *Nature*, **395**, issue 6704, 743–744, 1998.

57. Putirka, K., Melting depths and mantle heterogeneity beneath Hawaii and the East Pacific Rise: Constraints from Na/Ti and rare earth element ratios, *J. Geophys. Solid Earth*, **104**, issue B2, 2817–2829, 1999.

58. Putirka, K., Clinopyroxene plus liquid equilibria to 100 kbar and 2450 K, *Contrib. Miner. Petrol.*, **135**, issue 2–3, 151–163, 1999.

59. Wyllie, P.J., Experimental petrology of upper mantle materials, process and products, *J. Geodyn.*, **20**, issue 4, 429–468, 1995.

60. Leitch, A.M., M.J. Cordery, G.F. Davies, and I.H. Campbell, Flood basalts from eclogite-bearing mantle plumes, *S. Afr. J. Geol.*, **100**, 4, 311–318, 1997.

61. Hofmann, A.W., Mantle geochemistry: the message from oceanic volcanism, *Nature*, **385**, 6613, 219–229, 1997.

62. D'Orazio, M., S. Agostini, F. Mazzarini, F. Innocenti, P. Manetti, M.J. Haller, and A. Lahsen, The Palil Aike Volcanic Field, Patagonia: slab-window magmatism near the tip of South America, *Tectonophysics*, **321**, 4, 407–427, 2000.

63. Puzankov, Yu.M., Geochemistry of Cenozoic basite megmatism over "hot spots", *Geokhimiya*, 9, 941–949, 1999.

64. Cscerepes, L., and D.A. Yuen, On the possibility of second type of mantle plume, *Earth Planet. Sci. Lett.*, **183**, 61–71, 2000.

65. Humphreys, E.D., K.G. Dueker, D.L. Schutt, and R.B. Smith, Beneath Yellowstone: Evaluating Plume and Nonplume Models Using Teleseismic Images of the Upper Mantle, *GSA Today*, **10**, 123, 1–7.

66. Rasskazov, S.V., N.A. Logachev, and A.V. Ivanov, Correlation of Late Cenozoic tectonic and mantle events in Baikal Rift Zone and events in southeast of Eurasian Plate, *Geotektonika*, 4, 25–40, 1998.

67. Kulakov, I.Yu., S.A. Tychkov, and S.I. Keselman, Three dimension structure of lateral heterogeneity in *P*-velocities in the upper mantle of the southern margin of Siberia and its preliminary geodynamic interpretation, *Tectonophysics*, **241**, 239–257, 1995.

68. Kulakov, I.Yu., Three-dimensional seismic inhomogeneities beneath the Baikal region according to teleseismic and local tomography, *Geologiya i Geofizika (Russian Geology and Geophysics)*, **40**, 3, 317–331(317–329), 1999.

69. Touret, J.-C., Volcanic geomorphology — an overview, *Earth Sci. Revs.*, **47**, 95–131, 1999.

Editorial responsibility: V.N. Sharapov Received 29 January 2002